Imaging Oxysterols in Mouse Brain by On-Tissue Derivatisation – Robotic Micro-Liquid-Extraction Surface Analysis – Liquid Chromatography Mass Spectrometry

Eylan Yutuc[1], Roberto Angelini[1], Mark Baumert[2], Natalia Mast[3], Irina Pikuleva[3], Jillian Newton[4], Malcolm R Clench[4], David Skibinski[1], Owain W Howell[1], Yuqin Wang[1], William J Griffiths[1]

[1]Swansea University Medical School, ILS1 Building, Singleton Park, Swansea, SA2 8PP, Wales, UK.

[2]Advion Limited, Harlow Enterprise Hub, Edinburgh Way, Harlow, Essex, CM20 2NQ, UK.

[3]Department of Ophthalmology and Visual Sciences, Case Western Reserve University, Cleveland, OH, USA.

[4]Centre for Mass Spectrometry Imaging, Biomolecular Research Centre, Sheffield Hallam University, Howard Street, Sheffield, S1 1WB, UK.

Abstract

Oxysterols are bioactive metabolites of cholesterol and of its precursors. Although they are known to be present in brain their distribution in brain is poorly defined. The current study describes the exploitation of on-tissue enzyme-assisted derivatisation with micro-liquid-extraction for surface analysis and nano-liquid chromatography - mass spectrometry for the imaging of oxysterols in tissue slices (10 µm) of mouse brain. 24S-Hydroxycholesterol (24S-HC), derived from cholesterol through oxidation by the enzyme CYP46A1, was found to be the most abundant oxysterol in all brain regions, being at highest areal density in striatum (1.71 ± 0.27 ng/mm^2, mean ± SD, n = 3 animals) and in thalamus (1.75 ± 0.45 ng/mm^2) and at lowest levels in the grey matter of the cerebellum (0.18 ± 0.06 ng/mm^2). The combined presence of acidic sterols, 3β,7α-dihydroxycholest-5-en-(25R)26-oic and 7α-hydroxy-3-oxocholest-4-en-(25R)26-oic acid, was defined in all regions being most abundant in grey matter of cerebellum (0.02 ± 0.01 ng/mm^2), while 7-oxocholesterol was ubiquitously present at low levels (<0.01 ng/mm^2). By analysis of brain tissue of the *Cyp46a1* knockout mouse we confirmed the almost complete absence of 24S-HC and we are able to detect other oxysterols including 24R-hydroxycholesterol, which is most abundant in white matter of the cerebellum (0.02 ± 0.00 ng/mm^2), 25-hydroxycholesterol and the elusive 20S-hydroxycholesterol.

1. Introduction

Oxysterols are oxidised forms of cholesterol or of its precursors [Shroepfer 2000]. They are intermediates in steroid hormone and bile acid biosynthesis and possess diverse biological properties [Bjorkhem 2013, Luu 2016]. One of the most well studied oxysterols is 24S-hydroxycholesterol (24S-HC, cholest-5-ene-3β,24S-diol). In mammals it is mostly synthesised in neurons by the enzyme cytochrome P450 (CYP) 46A1 and acts as a transport form of cholesterol (Supplemental Figure S1) [Lund 1999, Bjorkhem 2006, Russell 2009]. Unlike cholesterol, 24S-HC can cross the blood brain barrier (BBB). 24S-HC is a ligand to the liver X receptors (LXRs) [Lehmann 1997], the β-form of which is highly expressed in brain [Wang 2002], a potent modulator of the *N*-methyl-D-aspartate receptors (NMDARs), glutamate-gated ion channels that are critical to the regulation of excitatory synaptic function in the central nervous system (CNS) [Paul 2013], and is also a modulator of cholesterol biosynthesis by interacting with the endoplasmic reticulum protein INSIG (insulin induced gene) and restricting transport and processing of SREBP-2 (sterol regulatory element-binding protein-2) to its active form as a master transcription factor for cholesterol biosynthesis [Radhakrishnan 2007, Wang 2008]. Despite its potent biological activity, little is known about levels of 24S-HC in distinct regions of brain [Heverin 2004, Mast 2017a]. This is also true of the cholestenoic acids, 3β,7α-dihydroxycholest-5-en-(25R)26-oic (3β,7α-diHCA) and 7α-hydroxy-3-oxocholest-4-en-(25R)26-oic (7αH,3O-CA) acids, also formed by enzymatic oxidation of cholesterol, and found in cerebrospinal fluid (CSF), the fluid that bathes the CNS [Theofilopoulos 2014, Saeed 2014]. 7αH,3O-CA has been suggested to provide an export route for (25R)26-hydroxycholesterol (26-HC, cholest-5-ene-3β,(25R)26-diol also called 27-hydroxycholesterol) which itself passes into the brain from the circulation, but does not accumulate in brain (see Supplemental Figure S1) [Heverin 2005, Meaney 2007]. 3β,7α-diHCA has been shown to be biologically active as a ligand to the LXRs and to be protective towards oculomotor neurons [Theofilopoulos 2014]. The location of neither acid has previously been defined in brain [Griffiths 2019].

The CNS represents a major repository of unesterified cholesterol in mammals, almost 25% of total body cholesterol is found in the CNS where it is present at a level of about 20 µg/mg (wet weight) [Dietschy 2004]. Much of that cholesterol is found in myelin sheaths of oligodendrocytes surrounding the axons of neurons, where it is turned over slowly (0.4%/day in mouse, 0.03% in human [Dietschy 2004]). A more metabolically active pool of cholesterol is located in intracellular structures such as the endoplasmic reticulum, Golgi apparatus and nucleus of neurons. Here turn-over is estimated at 20% per day in mouse [Dietschy 2004]. As cholesterol cannot cross the BBB essentially all cholesterol in brain is biosynthesised in brain. Inborn errors of cholesterol biosynthesis can result in neurodevelopmental disorders and retardation syndromes [Kanugo 2013].

Although cholesterol is the major source of oxysterols, its precursors can also be a source of these molecules [Javitt 2004, Griffiths 2017]. In fact, some cholesterol precursors have biological activity in their own right [Muse 2018]. Desmosterol (cholesta-5,24-dien-3β-ol), the immediate precursor of cholesterol in the Bloch arm of the cholesterol biosynthetic pathway, is both a ligand to the LXRs and also supresses SREBP-2 processing to its active form [Yang 2006, Radhakrishnan 2007]. While levels of cholesterol, desmosterol and other cholesterol precursors have been measured in brain homogenates, fewer studies have been performed to localise these sterols to distinct brain regions [Heverin 2004, Mast 2017a].

To understand better the importance in brain of sterols in general, and oxysterols in particular, it is necessary to correlate molecular concentrations with histology. This can be done by microdissection followed by homogenisation and sterol analysis by mass spectrometry (MS) [Heverin 2004, Mast 2017a]. However, with small laboratory animals this is not a simple task. An alternative method to

map sterol concentrations in brain is by exploiting mass spectrometry imaging (MSI). This technology pioneered for biological applications by Caprioli and colleagues in the USA [Norris 2013] and Spengler and colleagues in Europe [Spengler 2015], exploiting matrix-assisted laser desorption/ionisation (MALDI), has been widely used to image proteins, peptides and lipids in tissues [Berry 2011, Gessel 2014]. MALDI-MSI has been used to image lipids in brain [Trim 2008, Hankin 2011, Zemski Berry 2014], however, cholesterol and other sterols tend to be poorly ionised by conventional MALDI and are underrepresented in MALDI-MSI studies. To enhance ionisation other desorption methods have been employed, including nanostructure-initiator MS [Patti 2010], sputtered silver-MALDI [Xu 2015] and silver nanoparticle-MALDI [Roux 2016, Muller 2017]. Silver ions co-ordinate with carbon-carbon double bonds providing cationic adducts of sterols in the MALDI matrix.

MALDI-MSI has been used to image steroid hormones and steroidal drugs in tissue. To achieve this, researchers have utilised on-tissue derivatisation exploiting hydrazine reactions with carbonyl groups present in target analytes (e.g. Figure 1A) [Cobice 2013, 2016, 2018, Flinders 2015, Barré 2016, Shimma 2016]. Similar reactions have been utilised in "reactive-DESI" (desorption electrospray ionisation), an alternative ionisation technique that can be used for MSI [Badu-Tawiah 2012]. On-tissue derivatisation has also been used in combination with "liquid extraction for surface analysis" (LESA) technology [Cobice 2013, 2016, 2018], which is based on liquid micro-junction surface sampling [Van Berkel 2008], where solvent is deposited as a small volume droplet by a robotic sampling probe, i.e. pipette tip or capillary, onto a surface, aspirated back to the tip or capillary and the extract analysed by electrospray ionisation (ESI)-MS. For lipid analysis, the high organic content of the solvent can lead to solvent spreading and low spatial resolution. To minimise this, the sampling probe can be used to make a seal against the tissue surface, thereby preventing solvent spreading and minimising spot size (400 µm diameter) [Almeida 2015]. The advantage of on-tissue derivatisation in combination with LESA is that low abundance, or poorly ionised lipids i.e. steroids and oxysterols, can be targeted through derivatisation, allowing the observation of otherwise undetectable molecules, also giving sufficiently abundant ions for multi-stage fragmentation (MS^n) [Cobice 2013]. Cobice et al using a combination of on-tissue derivatisation, MALDI-MSI and LESA-MS^2 have monitored the distribution of corticosteroid in mouse brain tissue and confirmed 7-oxocholesterol (7-OC, 3β-hydroxycholest-5-en-7-one, also called 7-ketocholesterol) as a substrate for the enzyme 11β-hydroxysteroid dehydrogenase 1 (HSD11B1) and detected testosterone and 5α-dihydrotestosterone in mouse testis [Cobice 2013, 2016].

On-tissue derivatisation is problematic for sterols, oxysterols or steroids not possessing a carbonyl group. The hydroxy group can be targeted for derivatisation but this group is common to a wide range of biomolecules and this strategy provides little selectivity. An alternative approach, exploited for in-solution oxysterol analysis, is to utilise a bacterial cholesterol oxidase enzyme to specifically convert sterols with a 3β-hydroxy-5-ene or 3β-hydroxy-5α-hydrogen structure to 3-oxo-4-ene or 3-oxo-5α-sterols and then derivatise the 3-oxo group with the Girard hydrazine reagent to provide a charge-tag to the target molecule (Figure 1C) [Karu 2007, Roberg-Larsen 2014, Crick 2015]. This strategy is termed enzyme-assisted derivatisation for sterol analysis (EADSA). Oxysterols naturally possessing an oxo group, e.g. 7αH,3O-CA or 7-OC, can be derivatised in parallel in the absence of cholesterol oxidase. A challenge in oxysterol and sterol analysis is that the dominant sterol in mammals is cholesterol, usually being about a thousand-fold more abundant than other sterols or oxysterols. Thus, in the absence of chromatography, EADSA mass spectra are dominated by cholesterol. In the current study we describe how we have exploited on-tissue EADSA with micro-scale-LESA (µLESA) and nano-liquid chromatography (nano-LC) - MS(MS^n) for the imaging of oxysterols in rodent brain. We find 24S-HC to be the most abundant oxysterol in all brain regions, being at highest levels in striatum and thalamus and at lowest levels in grey matter of cerebellum. We are also able to definitively identify 3β,7α-diHCA

in brain, where it is most abundant in cerebellum. We confirm that 24S-HC is almost completely absent from brain of the *Cyp46a1* knockout mouse (*Cyp46a1*-/-), but low levels of 20S-hydroxycholesterol (20S-HC, cholest-5-ene-3β,20S-diol), 22R-hydroxycholesterol (cholest-5-ene-3β,22R-diol), 24R-hydroxycholesterol (24R-HC, cholest-5-ene-3β,24R-diol) and 25-hydroxycholesterol (25-HC, cholest-5-ene-3β,25-diol) are present in this mouse.

2. Results

2.1. Analytical Platform

The platform was designed to allow the MSI of oxysterols in tissue against a large background of cholesterol and other more readily ionised lipids. To meet this challenge, we have used on-tissue derivatisation (Figure 1) in combination with µLESA and nano-LC-MS(MS^n). Each of the system components required optimisation as described below.

2.1.1. On-Tissue EADSA

The protocol for on-tissue enzymatic oxidation of sterols (Figure 1) was adapted from the in-solution procedure using cholesterol oxidase enzyme in KH_2PO_4 buffer [Karu 2007, Crick 2015], the only difference being that the enzyme was sprayed onto tissue in buffer and then incubated at 37 °C in a humid chamber (11.9 cm x 8.2 cm x 8.5 cm, 30 mL water) rather than being in solution. In trial experiments, after a 1 hr incubation period at 37 °C there was no evidence for any non-oxidised sterol, only the 3-oxo-4-ene (see Supplemental Results 1.2.1.). The next step in the method was on-tissue derivatisation of oxo-containing sterols (Figure 1). Others have used Girard T (GT) hydrazine as the derivatising agent to react on-tissue with oxo-containing sterols/steroids [Cobice 2013, 2016, 2018, Flinders 2015, Barré 2016, Shimma 2016], however, based on our experience of using the Girard P (GP) reagent for in-solution derivatisation of oxysterols, GP hydrazine was preferred here [Karu 2007, Crick 2015]. A disadvantage of using GT hydrazine is that a major MS^2 fragment-ion is the $[M-59]^+$ species (Figure 1A) and the exact same neutral-loss is observed in the fragmentation of endogenous phosphocholine-containing lipids. With $[^2H_0]$GP the major MS^2 fragment-ion is $[M-79]^+$ and for $[^2H_5]$GP $[M-84]^+$, neutral-losses not common for other lipids. We sprayed GP reagent (6.3 mg/mL for $[^2H_5]$GP bromide or 5 mg/mL $[^2H_0]$GP chloride) in the same solvent as previously used for in-solution derivatisation (70% methanol 5% acetic acid) [Karu 2007, Crick 2015]. As in reported studies using the GT reagent [Cobice 2013, 2016, Barre 2016], it was essential to incubate the GP-coated tissue in a humid atmosphere to achieve efficient derivatisation. Initial tests in a dry atmosphere revealed no derivatisation of 3-oxo-4-ene substrates. Incubation in a humid chamber (12 cm x 12 cm x 7.2 cm) containing 30 mL of 50% methanol, 5% acetic acid at 37°C for 1 hr provided an efficient derivatisation environment with minimum lateral dispersion of analytes (see Supplemental Results 1.2.2. & 1.2.3 and Supplemental Figure S2). Increasing the volume or organic content of solution lead to lipid delocalisation, while reducing the volume and organic content provided less efficient derivatisation based on ion-current in µLESA-MS measurements. For comparison, Cobice et al sprayed GT hydrazine at 5 mg/mL in 80% methanol 0.1% trifluoroacetic acid and incubated in a sealed Petri dish containing 2 mL of water or in a sealed slide box at 80% humidity, for 60 min at 40 °C [Cobice et al 2013, 2016].

2.1.2. µLESA

Using conventional LESA, a pipette tip is positioned above the target surface and dispenses a µL-volume of extraction solvent to create a liquid micro-junction with the surface [Parson 2012]. After a sufficient time has elapsed for surface-liquid analyte extraction, solvent is then aspirated back to the tip. The pipette tip containing extract is then robotically transferred to a nano-ESI chip for MS analysis. Spot size using this format is typically $\geq$1 mm in diameter. The $LESA^{PLUS}$ configuration of the TriVersa Nanomate incorporates a 200 µm i.d. / 360 µm o.d. fused silica capillary replacing the pipette tip and when used with water-rich extraction solvents can improve spot size to $\leq$1 mm [Lamont 2017, Ryan 2018]. However, when using a 50% methanol solvent, as required here for extraction of derivatised sterols, we were unable to achieve this spot size as the surface tension required for a stable liquid micro-junction was not attainable. To overcome this problem, a 330 µm i.d. / 794 µm o.d. FEP

(fluorinated ethylene propylene) sleeve was attached to the fused silica capillary and used to make a direct seal with the tissue surface preventing spreading of the extraction solvent beyond the boundary of the sleeve (Supplemental Figure S3A). This gave a spot size of diameter <400 µm, as assessed by microscopic evaluation of tissue after liquid extraction (Supplemental Figure S3B). A 50% methanol extraction solvent was chosen to closely match the derivatisation solvent and loading phase used for the nano-LC injections (see below). The volume of solvent dispensed onto (more correctly, in contact with) tissue was optimised to maximise oxysterol extraction with an extraction time of 30 s, as assessed by MS ion-current for target oxysterols (e.g. 24S-HC), without compromising spatial resolution i.e. leaking of solvent through the tissue – FEP seal. The number of repeat extractions on the same spot was similarly optimised. The optimal conditions were a "dispensed volume" of 1 µL, an extraction time of 30 s, performed three times on the same spot.

Alternatively, Almeida et al have used LESA with a pipette tip to make a direct seal on-tissue for liquid extraction of lipids with organic solvents. They achieved a spot size of diameter 400 µm and directly analysed the extract by nano-ESI. Their extraction volume was 0.5 µL and extraction time 30 s [Almeida 2015].

2.1.3. Nano-LC

The nano-LC system was based on the reversed-phase LC system routinely used for oxysterol analysis after EADSA [Karu 2007, Crick 2015] and modified by Roberg-Larsen et al for nano-LC [Roberg-Larsen 2014]. By incorporating a reversed-phase trap column prior to the analytical column it was possible to trap GP-derivatised sterols and wash to waste unreacted GP reagent and polar analytes (Figure 2). After extraction of derivatised sterols by µLESA, loading on the trap column, and following a 13 min washing period, the trap column was back-flushed to the C_{18} analytical column. The gradient was optimised for analysis of oxysterols in brain allowing separation of the major oxysterol, 24S-HC, from the major sterol, cholesterol and its precursors desmosterol (cholesta-5,24-dien-3β-ol) and 7-dehydrocholesterol (7-DHC, cholesta-5,7-dien-3β-ol). To avoid cross-contamination between samples a column wash with an injection of 10 µL of 100% propan-2-ol and a fast gradient was performed between injection of samples. Carry-over into this wash for 24S-HC and cholesterol was <2%. This procedure eliminated carry-over of oxysterols into the next sample. The relative standard deviation of retention-time for 24S-HC was 0.3% ± 0.1% (mean ± SD) over five successive injections of derivatised brain tissue.

2.1.4. 24S-HC in Wild Type (WT) Mouse Brain

Previous studies using MS have defined concentrations of 24S-HC, the major oxysterol in mouse brain, to be of the order of 20 – 60 ng/mg (wet weight) [Ogundare 2010, Meljon 2014, Griffiths 2019, Mast 2017b]. For comparison, the concentration of cholesterol is in the range of 10 – 20 µg/mg [Dietschy 2004, Meljon 2014, Griffiths 2019], and after EADSA treatment, in the absence of chromatographic separation, cholesterol totally dominates the µLEASA-MS analysis of the mouse brain extract (Figure 3A). However, with the addition of nano-LC to give the µLESA-nano-LC-MS format, analysis of 400 µm diameter spot extracts of brain tissue give clear peaks for 24S-HC in reconstructed ion chromatograms (RICs) for the appropriate $[M]^+$ ion at *m/z* 539.4368 ± 10 ppm (Figure 3B, upper panel), in total ion chromatograms (TICs) for the transition 539.4→455.4→ (see Supplemental Figure S4B) and in the characteristic multiple-reaction monitoring (MRM) chromatograms 539.4→455.4→353.3 (Figure 3C, upper panel). The chromatographic peak doublet eluting at 27.57/28.36 in Figure 3B was confirmed to correspond to 24S-HC by exact mass measurement (Figure 3D) and from MS^3 ($[M]^+$→$[M\text{-}Py]^+$→) spectra (Figure 3E). The doublet is a consequence of *syn* and *anti* conformers of the GP-derivative. Relative quantification between spots was achieved using $[^2H_7]$24R/S-HC standard (central panels in

Figures 3B & C) sprayed on-tissue to an areal density of 1 ng/mm^2 (see below and Supplemental Methods 2.1.1).

2.1.5. EADSA-µLESA-nano-LC-MS

To assess the reproducibility of the EADSA-µLESA-nano-LC-MS technology six adjacent spots in the isocortical region of a single slice of mouse brain were analysed. The mean value of the peak area ratio 24S-HC : [$^2H_7$]24R/S-HC was 0.95 with a relative standard deviation of 8 %. This corresponds to an areal density of 24S-HC of 0.95 ± 0.08 ng/mm^2 (mean ± SD). Assuming that the endogenous concentration of 24S-HC did not vary across the six adjacent spots the reproducibility of the method is satisfactory. The reproducibility of the method was further assessed by analysing nine regions of interest from four closely cut slices from a single brain. The relative standard deviation for areal density in each individual region varied from 12.4 % for the striatum where the areal density of 24S-HC was high (1.41 ± 0.18 ng/mm^2, n = 4) to 46.3 % in the white matter of the cerebellum where the areal density of 24S-HC was low (0.19 ± 0.09 ng/mm^2, n = 4, Figure 4A).

The validity of using sprayed-on [$^2H_7$]24R/S-HC as an internal standard for quantification of oxysterols was assessed by spraying increasing concentration ratios of [$^2H_7$]24R/S-HC : [$^2H_7$]22S-HC onto six successive slices of brain tissue. A plot of average peak area ratio of [$^2H_7$]24R/S-HC : [$^2H_7$]22S-HC for three closely arranged spots from the same isocortical region on each slice, against spraying concentration of [$^2H_7$]24R/S-HC, keeping the concentration of [$^2H_7$]22S-HC constant, gave a straight line with R^2 > 0.999 (Supplemental Figure S5A). When this experiment was repeated but by plotting the average peak area ratio of [$^2H_7$]24R/S-HC : 24S-HC, where 24S-HC refers to the endogenous molecule, against spraying concentration of [$^2H_7$]24R/S-HC for closely arranged spots (n = 3) in the same region of interest on six successive slices, the result was a straight line of R^2> 0.992 (Supplemental Figure S5B). Assuming the concentration of endogenous 24S-HC does not vary across the six slices investigated in this study, or within the same region of interest, the results indicate that [$^2H_7$]24R/S-HC can be used as a reliable internal standard for quantification of endogenous 24S-HC.

2.2. Oxysterol in Different Regions of WT Mouse Brain

Nine brain regions of interest, i.e. isocortex, striatum, thalamus, hippocampus, midbrain, pons, medulla, cerebellum (grey matter) and cerebellum (white matter), were analysed by µLESA-nano-LC-MS (Figure 4).

2.2.1. 24S-HC

As is evident from Figures 4 & 5, 24S-HC is least abundant in the grey and white matter of the cerebellum (0.183 ± 0.063 ng/mm^2 and 0.234±0.073 ng/mm^2 respectively, n = 3 biological replicates, see also Supplemental Table S1) and most abundant in the striatum (1.711 ± 0.273 ng/mm^2) and thalamus (1.752 ± 0.449 ng/mm^2).

2.2.2. 3β,7α-diHCA, 7αH,3O-CA and 7-OC

Previous studies have suggested that 26-HC is imported into brain and converted in brain by a combination of enzymes, CYP27A1, CYP7B1 and HSD3B7 to 3β,7α-diHCA and 7αH,3O-CA (Supplemental Figure S1) [Heverin 2005, Meaney 2007, Theofilopoulos 2014, Iuliano 2015]. We thus generated RICs and TICs for the appropriate $[M]^+$ ion, *m/z* 569.4110 ± 10 ppm, and MS^3 transition $[M]^+ \rightarrow [M\text{-}Py]^+ \rightarrow$, i.e. 569.4→485.3→, for the acids (Figure S6A). When using EADSA with cholesterol oxidase the combination of the sterol acids with a 3β-hydroxy-5-ene i.e. 3β,7α-diHCA and native 3-oxo-4-ene structure i.e. 7αH,3O-CA is measured. The levels of the individual analytes are deconvoluted by repeat analysis on an adjacent section of brain tissue but in the absence of cholesterol oxidase

enzyme using [$^2H_7$]22S-HCO internal standard and [$^2H_0$]GP reagent (Supplemental Figure S7), in which case 7αH,3O-CA is measured but not 3β,7α-diHCA. However, when at low levels, the combined areal densities of 3β,7α-diHCA and 7αH,3O-CA can be measured more accurately than either of the individual species. The combination of 3β,7α-diHCA plus 7αH,3O-CA was evident at areal densities of 0.002 ± 0.002 - 0.018 ± 0.009 ng/mm^2 across the different regions of interest in mouse brain (see supplemental Table S1). In the absence of cholesterol oxidase treatment 7αH,3O-CA was detected in only some analysis at very low levels (0.001 ± 0.001 - 0.003 ± 0.001ng/mm^2) leading to values for the deconvoluted acid (3β,7α-diHCA) in the range of 0.00 ± 0.00 - 0.02 ± 0.01 ng/mm^2. For each of the individual brains analysed the combined acids and deconvoluted acids were most abundant in the grey matter of the cerebellum (Figure 5B and Supplemental Figure S8). For the three biological replicates the combined acids were found to be significantly (P<0.05) most abundant in the grey matter of the cerebellum (Figure 5B, see also supplemental Table S2).

7-OC can be formed from 7-DHC in a CYP7A1 catalysed reaction [Shinkyo 2011], or alternatively from cholesterol via free radical mediated reactions [Murphy 2008]. GP reagent will react with 7-OC in the absence of added cholesterol oxidase (Figure 1B). It is distributed ubiquitously across the brain at low levels (0.002 ± 0.002 – 0.004 ± 0.006 ng/mm^2). 7O-C has previously been detected in brain using Girard derivatisation and LESA-MS [Cobice 2013].

2.3. Oxysterols in Cyp46a1-/- Mouse Brain

2.3.1. 24S-HC, 24R-HC, 20S-HC and 12α-HC

In the WT mouse, the high areal density of 24S-HC (0.183 ± 0.063 - 1.752 ± 0.449 ng/mm^2) compared to other oxysterols makes the identification of any minor (<0.01 ng/mm^2) or closely eluting oxysterols difficult. To overcome this problem, we have taken advantage of brain tissue from the *Cyp46a1-/-* mouse which is reported to be almost completely devoid to 24S-HC [Lund 2003, Meljon 2014, Mast 2017b]. Analysis of the same brain regions as for WT mouse confirmed an almost complete absence of 24S-HC in the *Cyp46a1-/-* animal (Figure 3B-C) but revealed minor amounts of 25-HC (0.005 ± 0.002 - 0.023 ± 0.034 ng/mm^2) and 24R-HC (0.004 ± 0.002 – 0.023 ± 0.001 ng/mm^2, Figure S4B, see also Figure S9). Although there was some variation in absolute concentrations in different mice, 24R-HC was at highest concentration in the cerebellum of each mouse (Figure 5C, see also Supplemental Table S2), 25-HC was more ubiquitously dispersed (Figure S8 and Supplemental Table S1). Both of these oxysterols were detected at low levels in an earlier study of homogenised *Cyp46a1-/-* mouse brain, as was an unknown hydroxycholesterol eluting later than the second peak of 24R-HC. Here we again observe low levels of this oxysterol (0.007 ± 0.005 - 0.012 ± 0.006 ng/mm^2) which we have previously assigned, based on retention time and MS^3 spectra, to be 12α-hydroxycholesterol (12α-HC, Figure S9) [Griffiths 2019]. Careful interrogation of the MS^3 spectra recorded prior to the elution of 25-HC indicate the presence of not only trace quantities of 24S-HC (detected but not quantified, Figure S9A), but also of the elusive 20S-HC [Roberg-Larsen 2014]. 20S-HC gives a unique MS^3 spectrum where the fragment-ion *m/z* 327.2 is abundant (Figure S9A, B & G). By generating an MRM chromatogram for the transition *m/z* 539.4→455.4→327.2 this oxysterol is highlighted, although appearing as a shoulder on the leading edge of the 25-HC peak in the RIC for the [M]$^+$ ion (Figure 9A).

When the authentic standard of [$^2H_0$]GP-derivatised 20S-HC was spotted on mouse brain tissue it eluted with an identical retention time to the [$^2H_5$]GP derivatised endogenous molecule and the MS^3 spectra of the standard and endogenous molecule were very similar. There were some small differences in the spectra as a consequence of the co-elution of isomeric oxysterols from tissue. However, an intense fragment-ion at *m/z* 327.2 is unique to 20S-HC. 20S-HC has previously been

reported to be present in rat brain and human placenta [Lin 2003]. Here we confirm it presence also in mouse brain and provide its approximate quantification.

2.3.2. 7α,26-diHC and 7α,26-diHCO

7α,(25R)26-Dihydroxycholesterol (7α,26-diHC, cholest-5-ene-3β,7α(25R)26-triol) and 7α,(25R)26-dihydroxycholest-4-en-3-one (7α,26-diHCO) represent potential precursors of 7α-hydroxycholestenoic acids in brain (Supplemental Figure S1). Although the current LC gradient was not optimised with these two oxysterols in mind, their presence is defined by appropriate chromatographic peaks and by MS^3 spectra consistent with their structures (Figure S10). However, the additional presence of 7α,24S-dihydroxy and 7α,25-dihydroxy isomers and of the 7α,(25S)26-dihydroxy epimers, not separating from the 7α,(25R)26-dihydroxy isomer in the current system, cannot be ruled out. The levels of the dihydroxysterols are low in brain (0.001 ± 0.001 - 0.004 ± 0.004 ng/mm^2, Figure S10 A & B).

2.3.3. *3β,7α-diHCA and 7αH,3O-CA*

The combined areal densities of 3β,7α-diHCA and 7αH,3O-CA can be measured more accurately than either of the individual species. As with the WT mice, the combined acids were consistently most abundant in the grey matter of the cerebellum of the *Cyp46a1-/-* mice (0.013 ± 0.014 ng/mm^2, Figure S8, see also Figure S10 C – F), although again there was some mouse to mouse variation in areal density.

2.4. Cholesterol and its Precursors in WT Mouse Brain

Earlier studies have shown that the cholesterol content of whole brain does not differ significantly between WT and *Cyp46a1-/-* animals [Lund 2003, Meljon 2014, Mast 2017b] this was explained by a reduction of cholesterol synthesis compensating for reduced metabolism in the *Cyp46a1-/-* animals.

In the current study focus was on oxysterols rather than on cholesterol and its precursors. Never-the-less, it was possible to make approximate measurements for cholesterol and the sum of its precursors 7-DHC and desmosterol. For more precise and accurate measurements, it will be necessary to optimise the chromatography to separate the latter isomers and to reduce tailing of highly abundant cholesterol (Supplemental Figure S4A). Levels of cholesterol were of the order of 350 – 820 ng/mm^2 and of 7-DHC plus desmosterol 2 – 4 ng/mm^2. No statistically significant differences were found in areal densities between WT and *Cyp46a1-/-* brain regions. Cholest-4-en-3-one has been found to be present in brain of Alzheimer's disease sufferers and at lower levels in control brain samples [Puglielli 2005]. Here we detect cholest-4-ene-3-one in all regions of mouse brain at areal densities in the region of 0.15 – 0.32 ng/mm^2 in both WT and *Cyp46a1-/-* animals.

2.5. Application of MALDI-MSI for Cholesterol Analysis

As an alternative to µLESA-nano-LC-MS for the MSI of cholesterol we have explored the possibility of exploiting MALDI-MSI. Using on-tissue EADSA in a similar manner to that employed with µLESA, it was possible to image the $[M]^+$ ion of GP-derivatised cholesterol (Figure 6).

3. Discussion

In the current work we have defined a methodology for the MSI of oxysterols in mouse brain using EADSA and µLESA-nano-LC-MS. This method compliments MALDI-MSI methods, also based on EADSA, being concurrently developed for cholesterol and its precursors in our laboratory. The major oxysterol in brain is 24S-HC [Björkhem 2006, 2013]. Here we find it to be most abundant in the striatum and thalamus and least abundant in the cerebellum. 24S-HC is formed from cholesterol by the enzyme CYP46A1 expressed in neurons localised to multiple sub-regions of brain [Lund 1999]. In most studies, 24S-HC is analysed in whole brain homogenates being found at concentrations of 20 – 60 ng/mg. Our values of 0.183 – 1.752 ng/mm translate to 18 – 171 ng/mg assuming efficient extraction from the 10 µm thick tissue sections and nimimal desiccation during tissue storage.

Cholesterol is the most abundant sterol in brain, being about 10^3 more abundant that 24S-HC. In the absence of derivatisation, or chelation with Ag^+, cholesterol is barely detectable in most MSI experiments [Spengler 2015], and to date oxysterols, with the exception of 7-OC [Cobice 2013], and cholestenoic acids have not been imaged in brain. However, following EADSA, cholesterol provides the most abundant signal in MSI experiment of brain tissue (Figure 3A) and 24S-HC is clearly defined at areal densities of low ng/mm^2 by µLESA-nano-LC-MS (Figure 3B). The sensitivity of the system extends down to areal densities below 0.01 ng/mm^2, at which levels dihydroxysterols and cholestenoic acids are found (Supplemental Table S1).

The spatial resolution and spot size available with the µLESA format (400 µm spot diameter), is considerably inferior to that available with MALDI-MSI (50 µm laser spot diameter). However, µLESA can be coupled with LC, offering isomer separation, essential for oxysterol analysis of tissue surface, where resolution of endogenous oxysterols from those generated *ex vivo* by oxidation in air is required. MALDI can be linked with ion-mobility separation and MSI, but in experiments performed to date we have been unable to separate different oxysterol isomers. A disadvantage with the µLESA-nano-LC-MS format adopted here is chromatographic run time, with each spot taking approximately 1 hr to analyse. This could be reduced by increasing LC flow-rate and column diameter from a nano-scale to a more conventional scale, where 15 min run times are more typical [Karu 2007, Crick 2015]. However, increased flow-rate will come with the penalty of reduced sensitivity, due to the concentration dependency of ESI. This is unlikely to be an issue for 24S-HC but may well be for less abundant oxysterols.

It is interesting to compare the distribution of the most abundant oxysterols and cholestenoic acids measured here with the expression of genes coding for their biosynthetic enzymes, as detailed in the Allen Mouse Brain Atlas [Lein 2007]. According the Allen Mouse Brain Atlas the expression *Cyp46a1*, coding cholesterol 24S-hydroxylase, is highest in striatum and thalamus and lowest in cerebellum, which reflects the patterns of 24S-HC abundance measured here [Lein 2007] (see also Supplemental references). The gene *Cyp27a1* coding the enzyme required to introduce a hydroxy and then carboxylate group at C-26 of cholesterol was of highest expression in the cerebellum [Lein 2007], which is in agreement with data generated here, finding cholestenoic acids to be most abundant in cerebellum.

24S-HC is by far the most abundant oxysterol in mouse brain [Meljon 2014, Mast 2017b, Griffiths 2019]. This makes analysis of low abundance isomers challenging. However, deletion of *Cyp46a1* removes the biosynthesis of 24S-HC almost completely, allowing measurement of closely eluting or low abundance isomers [Meljon 2014]. In the current study we were able to image 24R-HC, the epimer of 24S-HC, which is found to be of most abundance in cerebellum and to detect other isomers 12α-HC, 25-HC and the elusive 20S-HC. 22R-HC was also detected but at levels below the limit of

quantification. The enzymes required to biosynthesise 24R-HC and 20S-HC from cholesterol are unknown. The abundance of 24R-HC in cerebellum of the *Cyp46a1-/-* mouse does suggest CYP27A1 to be the relevant cholesterol hydroxylase, but this is unlikely as 24R-HC is present in brain of the *Cyp27a1-/-* mouse [Griffiths 2019]. CYP3A11 is also a sterol 24R-hydroxylase and could perhaps convert cholesterol to 24R-HC in brain. It is however, predominantly expressed in cortex [Lein 2007]. CYP11A1 is the cholesterol 22R-hydroxylase required for neurosteroid biosynthesis and has been shown to be expressed in mouse brain [Chiang 2011]. It first hydroxylates cholesterol at position C-22R then at C-20, then cleaves the bond between these two carbons to generate pregnenolone. Besides being the enzyme responsible to generate 22R-HC from cholesterol, it may also be the catalyst for formation of 20S-HC from cholesterol, although evidence for this suggestion is lacking. There is only one previous report of the identification of 20S-HC in rodents or human [Lin 2003]. However, 20S-HC is of considerable biological interest being a ligand to the G protein-coupled receptor (GPCR) smoothened (SMO), an integral receptor protein in the hedgehog (Hh) signalling pathway, important for determining cell fate during development [Dwyer 2007, Nachtergaele 2012, Nedelcu 2013].

In summary, application of EADSA with LESA-µLESA-nano-LC-MSI allows spatial location of oxysterols and cholestenoic acids in mouse brain. Through exploitation of the *Cyp46a1-/-*, where the biosynthesis of 24S-HC is almost completely eliminated, other minor oxysterols are revealed. To compliment EADSA-µLESA-nano-LC-MSI we are developing EADSA in combination with MALDI-MSI. We find this ideal for imaging cholesterol at high spatial resolution.

4. Material and Methods

4.1. Common Experimental Design

The objective of the current study was to develop a MSI method suitable for the low-level quantitative determination of different oxysterols, including cholestenoic acids, in different regions of mouse brain.

4.1.1. Chemicals and Reagents

HPLC grade methanol and water were from Fisher Scientific (Loughborough, UK). Glacial acetic and formic acids were purchased from VWR (Lutterworth, UK). [25,26,26,26,27,27,27-$^2H_7$]22S-hydroxycholesterol ([$^2H_7$]22S-HC, [25,26,26,26,27,27,27-$^2H_7$]cholest-5-ene-3β,22S-diol), [25,26,26,26,27,27,27-$^2H_7$]22R-hydroxycholesterol ([$^2H_7$]22R-HC, [25,26,26,26,27,27,27-$^2H_7$]cholest-5-ene-3β,22R-diol), [25,26,26,26,27,27,27-$^2H_7$]24R/S-hydroxycholesterol ([$^2H_7$]24R/S-HC, [25,26,26,26,27,27,27-$^2H_7$]cholest-5-ene-3β,24R/S-diol) and [25,26,26,26,27,27,27-$^2H_7$]cholesterol were from Avanti Polar Lipids (Alabaster, AL). [25,26,26,26,27,27,27-$^2H_7$]22S-hydroxycholest-4-en-3-one ([$^2H_7$]22S-HCO) and [25,26,26,26,27,27,27-$^2H_7$]22R-hydroxycholest-4-en-3-one ([$^2H_7$]22R-HCO) were prepared from [$^2H_7$]22S-HC and [$^2H_7$]22R-HC, respectively, as described in Crick et al [Crick 2015]. Cholesterol oxidase from *Streptomyces sp.* and potassium dihydrogen phosphate were from Sigma-Aldrich, now Merck (Dorset, UK). [$^2H_0$]Girard P ([$^2H_0$]GP) was from TCI Europe (Zwijndrecht, Belgium). [$^2H_5$]GP was synthesised as described by Crick et al [Crick 2014, Crick 2015]. Alpha-cyano-4-hydroxycinnamic acid (CHCA) was from Sigma-Aldrich (Dorset, UK)

4.1.2. Tissue Sectioning

Mouse brain was from male 4-month-old *Cyp46a1-/-* and wild type (WT *Cyp46a1+/+*, C57BL/6J;129S6/SvEv) littermates as detailed in [Mast 2017b]. Fresh frozen tissue, mounted in OCT (optimal cutting temperature compound), was cryo-sectioned using a Leica Cryostat CM1900 (Leica Microsystems, Milton Keynes, UK) at a chamber temperature of -16°C into 10 µm-thick sections which were thaw-mounted onto glass microscope slides and stored at -80°C until use. Luxol Fast Blue and Cresyl Violet staining was performed on tissue sections adjacent to sections analysed by MSI. For MALDI-MS, ITO (indium tin oxide) coated glass slides were from Diamond Coatings (Halesowen, UK).

4.1.3. Deposition of Internal Standard and On-Tissue EADSA

Frozen tissue sections were dried in a vacuum desiccator for 15 min after which an internal standard mixture of [$^2H_7$]24R/S-HC (5 ng/µL), [$^2H_7$]22S-HC (1 ng/µL), [$^2H_7$]22S-HCO (1 ng/µL), and in some experiments [$^2H_7$]22R-HCO (1 ng/µL), in ethanol were sprayed from a SunCollect automated pneumatic sprayer (SunChrom, Friedrichsdorf, Germany supplied by KR Analytical Ltd, Cheshire, UK) at a flow rate of 20 µL/min at a linear velocity of 900 mm/min with 2 mm line distance and Z position of 30 mm in a series of 18 layers. The resulting density of the deuterated standard were, 1 ng/mm^2 for 24R/S-HC, and 0.2 ng/mm^2 for each of [$^2H_7$]22S-HC, [$^2H_7$]22S-HCO and [$^2H_7$]22R-HCO (see Supplemental Methods 2.1.1.). The sprayer was thoroughly flushed with about 2 mL of methanol after which cholesterol oxidase (0.264 units/mL in 50 mM KH_2PO_4 pH7) was sprayed for 18 layers. The first layer was applied at 10 µL/min, the second at 15 µL/min, then all the subsequent layers at 20 µL/min to give an enzyme density of 0.05 munits/mm^2. Thereafter, the enzyme-coated slide was placed on a flat dry bed in a sealed pipette-tip box (11.9 cm x 8.2 cm x 8.5 cm) above 30 mL of warm water (37 °C), then incubated at 37°C for 1 hr. After which, the slide was removed and dried in a vacuum desiccator for 15 mins. [$^2H_5$]GP (6.3 mg/mL in 70% methanol with 5% acetic acid) was sprayed on the dried slide with the same spray parameters as used for spraying cholesterol oxidase. The resulting GP density was

1.21 µg/mm^2. The slide was then placed on a flat dry table in a covered glass chamber (12 cm x 12 cm x 7.2 cm) containing 30 mL of pre-warmed (37 °C) 50% methanol, 5% acetic acid and incubated in a water bath at 37°C for 1 hr. The slide was removed and dried in a vacuum desiccator until nano-LC-MS analysis. To analyse sterols containing a naturally occurring oxo group the cholesterol oxidase spray step was omitted and [$^2H_0$]GP (5 mg/mL in 70% methanol with 5% acetic acid) used as the derivatisation agent.

For MALDI-MSI experiments the above procedure was slightly modified as described in Supplemental Methods 2.2.

4.2. µLESA-nano-LC-MSI

4.2.1. Robotic µLESA

Derivatised oxysterols present in 10 µm thick slices of brain tissue were sampled using a TriVersa Nanomate (Advion, Ithaca, NY) with a modified capillary extraction probe (LESA^{PLUS}). The Advion ChipsoftX software was used to capture an optical image of the prepared slide on a flatbed scanner prior to analysis. The same software was also used to define extraction points on the tissue prior to analysis. A 330 µm i.d. / 794 µm o.d. FEP (a copolymer of hexafluoropropylene and tetrafluoroethylene) sleeve was attached to a 200 µm i.d. / 360 µm o.d. fused silica capillary held in the mandrel of the Advion TriVersa Nanomate, this created a seal when in contact with tissue preventing the dispersion of extraction solvent (50% methanol) and limiting the sampling area to the internal diameter of the FEP sleeve (see Supplemental Figure S3).

Three µL of extraction solvent was aspirated into the capillary from the solvent reservoir (R3 – R4 in Figure 2), the mandrel moved robotically to an exact tissue location and 1 µL of solvent dispensed on-tissue and held for 30 s before being aspirated back into the capillary. The mandrel moved once again, and the extract was dispensed into a well of a 384-well plate. The process was repeated twice more with extract dispensed into the same well, before the combined extract was injected via the extraction probe into the sample loop of the nano-LC system (see below). The entire procedure was then repeated on a new extraction point. Multiple points were analysed to build up an oxysterol image of brain tissue.

4.2.2. Nano-LC-MS(MS^n)

Nano-LC separations were performed on an Ultimate 3000 UHPLC system (Dionex, now Thermo Scientific, Hemel Hempstead, UK). The µLESA extract was delivered from the sample loop onto a trap column (HotSep Tracy C_8, 5 µm 100 Å, 5 mm x 0.3 mm, Kinesis Ltd, Bedfordshire, UK) using a loading solvent of 50% methanol, 0.1% formic acid at a flow-rate of 5 µL/min. The eluent from the trap column containing unreacted GP reagent was delivered to waste (Figure 2). After 13 min the trap column was switched in-line with the analytical column (ACE C_{18}, 3 µm 100 Å, 100 mm x 0.1 mm, Aberdeen, Scotland) and a gradient delivered by the binary nanopump at 0.6 µL/min. Mobile phase A consisted of 50% methanol, 0.1% formic acid and mobile phase B consisted of 95% methanol, 0.1% formic acid. At 13 min, the time of valve switching, the proportion of B was 40 %, and was raised to 60% B over the next 5 min and maintained at 60% B for 5 min, then raised again to 95% B over 5 min and maintained at 95% B for a further 38 min before being reduced to 20% B in 1 min (run time 67 min) and the column re-equilibrated for 11 min. The trap-column was switched out of line at 67 min and re-equilibrated for 11 min with 50% methanol, 0.1% formic acid prior to the next injection (Supplemental Figure 3C). The column eluent was directly infused into an Orbitrap Elite mass spectrometer (Thermo Scientific, Hemel Hempstead, UK) using the Nanomate chip-based nano-ESI (Advion, Ithaca, NY) set at between 1.7 kV and 2.0 kV chip voltage. To avoid cross-contamination

between samples a column wash with injection of 10 µL of 100% propan-2-ol and a fast gradient of 36 min was performed between injections of tissue extracts. The 100% propan-2-ol "plug" was delivered to the trap column and washed for 5 min before being switched in-line with the analytical column, which during this period was washed independently by raising the proportion of B from 20% to 95%. With the two columns in-line the proportion of B was maintained at 95% B 19 min after which it returned to 20% within 1 min. The trap column was then switched off-line and both columns equilibrated for a further 11 min before the next sample was injected. The gradients are illustrated in Supplemental Figure S3.

For each injection five scan events were performed: one high resolution scan (240,000 full-width at half maximum height definition at *m/z* 400) in the Orbitrap analyser in parallel to four MS^3 scan events in the linear ion-trap. Quantification was by isotope dilution using tissue-coated isotope-labelled standard. MS^3 scans were for the transitions $[M]^+ \rightarrow [M\text{-}Py]^+ \rightarrow$, where Py is the pyridine group of the GP-derivative.

4.2.3. Quantification

To achieve reliable quantitative measurements known amounts of isotope labelled internal standard $[^2H_7]$24R/S-HC (for use with cholesterol oxidase) and $[^2H_7]$22S-HCO (for use in the absence of cholesterol oxidase) were sprayed on-tissue prior to the EADSA process. This procedure corrects for variation in surface extraction, injection volume, and MS response. Quantification was made from $[M]^+$ ion signals in appropriate RICs. Approximate quantification of 20S-HC was performed by utilising the MRM $[M]^+ \rightarrow [M\text{-}Py]^+ \rightarrow 327.2$ transition and quantifying against the $[M]^+ \rightarrow [M\text{-}Py]^+ \rightarrow 353.3$ for $[^2H_7]$24R/S-HC (see Supplemental Figure S9G).

4.3. Statistics

One-way ANOVA, followed by Tukey's corrected multiple comparisons test with a single pooled variance, were performed to determine statistical difference of sterol areal densities between different regions of mouse brain using GraphPad Prism 7.02 software (GraphPad Software, Inc, CA, USA). A *P*-value of less than 0.05 was considered statistically significant. $P<0.05$, *; $P<0.01$, **; $P<0.001$, ***; $P<0.0001$. Whiskers on bar graphs represent standard deviation (SD).

Acknowledgements

This work was supported by the UK Biotechnology and Biological Sciences Research Council (BBSRC, grant numbers BB/I001735/1 and BB/N015932/1 to WJG, BB/L001942/1 to YW). RA holds a Sêr Cymru Fellowship supported by the Welsh Government and the European Regional Development Fund. Work in IP's laboratory is supported by the National Institute of Health (grant number R01 GM062882). Members of the European Network for Oxysterol Research (ENOR, https://www.oxysterols.net/) are thanked for informative discussions. Dr Ruth Andrew is thanked for advice on performing on-tissue derivatisation and Drs Hanne Røberg-Larsen and Steven Wilson are thanked for information regarding nano-LC separations.

References

Oxysterols: modulators of cholesterol metabolism and other processes. **Schroepfer GJ Jr**. Physiol Rev. 2000 Jan;80(1):361-554.
Five decades with oxysterols. **Björkhem I**. Biochimie. 2013 Mar;95(3):448-54.
Oxysterols: Old Tale, New Twists. **Luu W**, Sharpe LJ, Capell-Hattam I, Gelissen IC, Brown AJ. Annu Rev Pharmacol Toxicol. 2016;56:447-67.
cDNA cloning of cholesterol 24-hydroxylase, a mediator of cholesterol homeostasis in the brain. **Lund EG**, Guileyardo JM, Russell DW. Proc Natl Acad Sci U S A. 1999 Jun 22;96(13):7238-43.
Crossing the barrier: oxysterols as cholesterol transporters and metabolic modulators in the brain. **Björkhem I**. J Intern Med. 2006 Dec;260(6):493-508.
Cholesterol 24-hydroxylase: an enzyme of cholesterol turnover in the brain. **Russell DW**, Halford RW, Ramirez DM, Shah R, Kotti T. Annu Rev Biochem. 2009;78:1017-40.
Activation of the nuclear receptor LXR by oxysterols defines a new hormone response pathway. **Lehmann JM**, Kliewer SA, Moore LB, Smith-Oliver TA, Oliver BB, Su JL, Sundseth SS, Winegar DA, Blanchard DE, Spencer TA, Willson TM. J Biol Chem. 1997 Feb 7;272(6):3137-40.
Liver X receptors in the central nervous system: from lipid homeostasis to neuronal degeneration. **Wang L**, Schuster GU, Hultenby K, Zhang Q, Andersson S, Gustafsson JA. Proc Natl Acad Sci U S A. 2002 Oct 15;99(21):13878-83.
The major brain cholesterol metabolite 24(S)-hydroxycholesterol is a potent allosteric modulator of N-methyl-D-aspartate receptors. **Paul SM**, Doherty JJ, Robichaud AJ, Belfort GM, Chow BY, Hammond RS, Crawford DC, Linsenbardt AJ, Shu HJ, Izumi Y, Mennerick SJ, Zorumski CF. J Neurosci. 2013 Oct 30;33(44):17290-300.
Sterol-regulated transport of SREBPs from endoplasmic reticulum to Golgi: oxysterols block transport by binding to Insig. **Radhakrishnan A**, Ikeda Y, Kwon HJ, Brown MS, Goldstein JL. Proc Natl Acad Sci U S A. 2007 Apr 17;104(16):6511-8.
The effect of 24S-hydroxycholesterol on cholesterol homeostasis in neurons: quantitative changes to the cortical neuron proteome. **Wang Y**, Muneton S, Sjövall J, Jovanovic JN, Griffiths WJ. J Proteome Res. 2008 Apr;7(4):1606-14.
Changes in the levels of cerebral and extracerebral sterols in the brain of patients with Alzheimer's disease. **Heverin M**, Bogdanovic N, Lütjohann D, Bayer T, Pikuleva I, Bretillon L, Diczfalusy U, Winblad B, Björkhem I. J Lipid Res. 2004 Jan;45(1):186-93.
Cytochrome P450 27A1 Deficiency and Regional Differences in Brain Sterol Metabolism Cause Preferential Cholestanol Accumulation in the Cerebellum. **Mast N**, Anderson KW, Lin JB, Li Y, Turko IV, Tatsuoka C, Bjorkhem I, Pikuleva IA. J Biol Chem. 2017a Mar 24;292(12):4913-4924.
Cholestenoic acids regulate motor neuron survival via liver X receptors. **Theofilopoulos S**, Griffiths WJ, Crick PJ, Yang S, Meljon A, Ogundare M, Kitambi SS, Lockhart A, Tuschl K, Clayton PT, Morris AA, Martinez A, Reddy MA, Martinuzzi A, Bassi MT, Honda A, Mizuochi T, Kimura A, Nittono H, De Michele G, Carbone R, Criscuolo C, Yau JL, Seckl JR, Schüle R, Schöls L, Sailer AW, Kuhle J, Fraidakis MJ, Gustafsson JÅ, Steffensen KR, Björkhem I, Ernfors P, Sjövall J, Arenas E, Wang Y. J Clin Invest. 2014 Nov;124(11):4829-42.
7α-hydroxy-3-oxo-4-cholestenoic acid in cerebrospinal fluid reflects the integrity of the blood-brain barrier. **Saeed A**, Floris F, Andersson U, Pikuleva I, Lövgren-Sandblom A, Bjerke M, Paucar M, Wallin A, Svenningsson P, Björkhem I. J Lipid Res. 2014 Feb;55(2):313-8.
Crossing the barrier: net flux of 27-hydroxycholesterol into the human brain. **Heverin M**, Meaney S, Lütjohann D, Diczfalusy U, Wahren J, Björkhem I. J Lipid Res. 2005 May;46(5):1047-52.
Novel route for elimination of brain oxysterols across the blood-brain barrier: conversion into 7alpha-hydroxy-3-oxo-4-cholestenoic acid. **Meaney S**, Heverin M, Panzenboeck U, Ekström L,

Axelsson M, Andersson U, Diczfalusy U, Pikuleva I, Wahren J, Sattler W, Björkhem I. J Lipid Res. 2007 Apr;48(4):944-51.
Additional pathways of sterol metabolism: Evidence from analysis of Cyp27a1-/- mouse brain and plasma. **Griffiths WJ**, Crick PJ, Meljon A, Theofilopoulos S, Abdel-Khalik J, Yutuc E, Parker JE, Kelly DE, Kelly SL, Arenas E, Wang Y. Biochim Biophys Acta Mol Cell Biol Lipids. 2019 Feb;1864(2):191-211.
Thematic review series: brain Lipids. Cholesterol metabolism in the central nervous system during early development and in the mature animal. **Dietschy JM**, Turley SD. J Lipid Res. 2004 Aug;45(8):1375-97.
Sterol metabolism disorders and neurodevelopment-an update. **Kanungo S**, Soares N, He M, Steiner RD. Dev Disabil Res Rev. 2013;17(3):197-210.
Oxysteroids: a new class of steroids with autocrine and paracrine functions. **Javitt NB**. Trends Endocrinol Metab. 2004 Oct;15(8):393-7.
Cholesterolomics: An update. **Griffiths WJ**, Abdel-Khalik J, Yutuc E, Morgan AH, Gilmore I, Hearn T, Wang Y. Anal Biochem. 2017 May 1;524:56-67.
Cell-specific discrimination of desmosterol and desmosterol mimetics confers selective regulation of LXR and SREBP in macrophages. **Muse ED**, Yu S, Edillor CR, Tao J, Spann NJ, Troutman TD, Seidman JS, Henke A, Roland JT, Ozeki KA, Thompson BM, McDonald JG, Bahadorani J, Tsimikas S, Grossman TR, Tremblay MS, Glass CK. Proc Natl Acad Sci U S A. 2018 Apr 9. pii: 201714518. doi: 10.1073/pnas.1714518115. [Epub ahead of print].
Sterol intermediates from cholesterol biosynthetic pathway as liver X receptor ligands. **Yang C**, McDonald JG, Patel A, Zhang Y, Umetani M, Xu F, Westover EJ, Covey DF, Mangelsdorf DJ, Cohen JC, Hobbs HH. J Biol Chem. 2006 Sep 22;281(38):27816-26.
Analysis of tissue specimens by matrix-assisted laser desorption/ionization imaging mass spectrometry in biological and clinical research. **Norris JL**, Caprioli RM. Chem Rev. 2013 Apr 10;113(4):2309-42.
Mass spectrometry imaging of biomolecular information. **Spengler B**. Anal Chem. 2015 Jan 6;87(1):64-82.
MALDI imaging of lipid biochemistry in tissues by mass spectrometry. **Berry KA**, Hankin JA, Barkley RM, Spraggins JM, Caprioli RM, Murphy RC. Chem Rev. 2011 Oct 12;111(10):6491-512.
MALDI imaging mass spectrometry: spatial molecular analysis to enable a new age of discovery. **Gessel MM**, Norris JL, Caprioli RM. J Proteomics. 2014 Jul 31;107:71-82.
Matrix-assisted laser desorption/ionisation mass spectrometry imaging of lipids in rat brain tissue with integrated unsupervised and supervised multivariant statistical analysis. **Trim PJ**, Atkinson SJ, Princivalle AP, Marshall PS, West A, Clench MR. Rapid Commun Mass Spectrom. 2008 May;22(10):1503-9.
MALDI mass spectrometric imaging of lipids in rat brain injury models. **Hankin JA**, Farias SE, Barkley RM, Heidenreich K, Frey LC, Hamazaki K, Kim HY, Murphy RC. J Am Soc Mass Spectrom. 2011 Jun;22(6):1014-21.
Spatial organization of lipids in the human retina and optic nerve by MALDI imaging massspectrometry. **Zemski Berry KA**, Gordon WC, Murphy RC, Bazan NG. J Lipid Res. 2014 Mar;55(3):504-15.
Nanostructure-initiator mass spectrometry (NIMS) imaging of brain cholesterol metabolites in Smith-Lemli-Opitz syndrome. **Patti GJ**, Shriver LP, Wassif CA, Woo HK, Uritboonthai W, Apon J, Manchester M, Porter FD, SiuzdakG. Neuroscience. 2010 Oct 27;170(3):858-64.
Profiling and Imaging Ion Mobility-Mass Spectrometry Analysis of Cholesterol and 7-Dehydrocholesterol in Cells Via Sputtered Silver MALDI. **Xu L**, Kliman M, Forsythe JG, Korade Z, Hmelo AB, Porter NA, McLean JA. J Am Soc Mass Spectrom. 2015 Jun;26(6):924-33.

Mass spectrometry imaging of rat brain lipid profile changes over time following traumatic brain injury. **Roux A**, Muller L, Jackson SN, Post J, Baldwin K, Hoffer B, Balaban CD, Barbacci D, Schultz JA, Gouty S, Cox BM, Woods AS. J Neurosci Methods. 2016 Oct 15;272:19-32.
Laser Desorption/Ionization Mass Spectrometric Imaging of Endogenous Lipids from Rat Brain Tissue Implanted with Silver Nanoparticles. **Muller L**, Baldwin K, Barbacci DC, Jackson SN, Roux A, Balaban CD, Brinson BE, McCully MI, Lewis EK, Schultz JA, Woods AS. J Am Soc Mass Spectrom. 2017 Aug;28(8):1716-1728.
Mass spectrometry imaging for dissecting steroid intracrinology within target tissues. **Cobice DF**, Mackay CL, Goodwin RJ, McBride A, Langridge-Smith PR, Webster SP, Walker BR, Andrew R. Anal Chem. 2013 Dec 3;85(23):11576-84
Spatial Localization and Quantitation of Androgens in Mouse Testis by Mass Spectrometry Imaging. **Cobice DF**, Livingstone DE, Mackay CL, Goodwin RJ, Smith LB, Walker BR, Andrew R. Anal Chem. 2016 Nov 1;88(21):10362-10367
Quantification of 11β-hydroxysteroid dehydrogenase 1 kinetics and pharmacodynamic effects of inhibitors in brain using mass spectrometry imaging and stable-isotope tracers in mice. **Cobice DF**, Livingstone DEW, McBride A, MacKay CL, Walker BR, Webster SP, Andrew R. Biochem Pharmacol. 2018 Feb;148:88-99.
The use of hydrazine-based derivatization reagents for improved sensitivity and detection of carbonyl containing compounds using MALDI-MSI. **Flinders B**, Morrell J, Marshall PS, Ranshaw LE, Clench MR. Anal Bioanal Chem. 2015 Mar;407(8):2085-94.
Derivatization Strategies for the Detection of Triamcinolone Acetonide in Cartilage by Using Matrix-Assisted Laser Desorption/Ionization Mass Spectrometry Imaging. **Barré FP**, Flinders B, Garcia JP, Jansen I, Huizing LR, Porta T, Creemers LB, Heeren RM, Cillero-Pastor B. Anal Chem. 2016 Dec 20;88(24):12051-12059.
Microscopic visualization of testosterone in mouse testis by use of imaging mass spectrometry. **Shimma S**, Kumada HO, Taniguchi H, Konno A, Yao I, Furuta K, Matsuda T, Ito S. Anal Bioanal Chem. 2016 Nov;408(27):7607-7615. Epub 2016 May 26. Erratum in: Anal Bioanal Chem. 2016 Nov;408(27):7881.
Reactions of microsolvated organic compounds at ambient surfaces: droplet velocity, charge state, and solvent effects. **Badu-Tawiah AK**, Campbell DI, Cooks RG. J Am Soc Mass Spectrom. 2012 Jun;23(6):1077-84.
Liquid microjunction surface sampling probe electrospray mass spectrometry for detection of drugs and metabolites in thin tissue sections. **Van Berkel GJ**, Kertesz V, Koeplinger KA, Vavrek M, Kong AN. J Mass Spectrom. 2008 Apr;43(4):500-8.
Quantitative spatial analysis of the mouse brain lipidome by pressurized liquid extraction surface analysis. **Almeida R**, Berzina Z, Arnspang EC, Baumgart J, Vogt J, Nitsch R, Ejsing CS. Anal Chem. 2015 Feb 3;87(3):1749-56.
Liquid chromatography-mass spectrometry utilizing multi-stage fragmentation for the identification of oxysterols. **Karu K**, Hornshaw M, Woffendin G, Bodin K, Hamberg M, Alvelius G, Sjövall J, Turton J, Wang Y, Griffiths WJ. J Lipid Res. 2007 Apr;48(4):976-87.
Highly automated nano-LC/MS-based approach for thousand cell-scale quantification of side chain-hydroxylated oxysterols. **Roberg-Larsen H**, Lund K, Vehus T, Solberg N, Vesterdal C, Misaghian D, Olsen PA, Krauss S, Wilson SR, Lundanes E. J Lipid Res. 2014 Jul;55(7):1531-6.
Quantitative charge-tags for sterol and oxysterol analysis. **Crick PJ**, William Bentley T, Abdel-Khalik J, Matthews I, Clayton PT, Morris AA, Bigger BW, Zerbinati C, Tritapepe L, Iuliano L, Wang Y, Griffiths WJ. Clin Chem. 2015 Feb;61(2):400-11.

Analysis of chloroquine and metabolites directly from whole-body animal tissue sections by liquid extraction surface analysis (LESA) and tandem mass spectrometry. **Parson WB**, Koeniger SL, Johnson RW, Erickson J, Tian Y, Stedman C, Schwartz A, Tarcsa E, Cole R, Van Berkel GJ. J Mass Spectrom. 2012 Nov;47(11):1420-8.
Integration of Ion Mobility MS_E after Fully Automated, Online, High-Resolution Liquid Extraction Surface Analysis Micro-Liquid Chromatography. **Lamont L**, Baumert M, Ogrinc Potočnik N, Allen M, Vreeken R, Heeren RMA, Porta T. Anal Chem. 2017 Oct 17;89(20):11143-11150.
Protein identification in imaging mass spectrometry through spatially targeted liquid micro-extractions. **Ryan DJ**, Nei D, Prentice BM, Rose KL, Caprioli RM, Spraggins JM. Rapid Commun Mass Spectrom. 2018 Mar 15;32(5):442-450.
Cerebrospinal fluid steroidomics: are bioactive bile acids present in brain? **Ogundare M**, Theofilopoulos S, Lockhart A, Hall LJ, Arenas E, Sjövall J, Brenton AG, Wang Y, Griffiths WJ. J Biol Chem. 2010 Feb 12;285(7):4666-79
Oxysterols in the brain of the cholesterol 24-hydroxylase knockout mouse. **Meljon A**, Wang Y, Griffiths WJ. Biochem Biophys Res Commun. 2014 Apr 11;446(3):768-74.
Transcriptional and post-translational changes in the brain of mice deficient in cholesterol removal mediated by cytochrome P450 46A1 (CYP46A1). **Mast N**, Lin JB, Anderson KW, Bjorkhem I, Pikuleva IA. PLoS One. 2017b Oct 26;12(10):e0187168.
Cholesterol metabolites exported from human brain. **Iuliano L**, Crick PJ, Zerbinati C, Tritapepe L, Abdel-Khalik J, Poirot M, Wang Y, Griffiths WJ. Steroids. 2015 Jul;99(Pt B):189-93.
Conversion of 7-dehydrocholesterol to 7-ketocholesterol is catalyzed by human cytochrome P450 7A1 and occurs by direct oxidation without an epoxide intermediate. **Shinkyo R**, Xu L, Tallman KA, Cheng Q, Porter NA, Guengerich FP. J Biol Chem. 2011 Sep 23;286(38):33021-8.
Cholesterol, reactive oxygen species, and the formation of biologically active mediators. **Murphy RC**, Johnson KM. J Biol Chem. 2008 Jun 6;283(23):15521-5.
Knockout of the cholesterol 24-hydroxylase gene in mice reveals a brain-specific mechanism of cholesterol turnover. **Lund EG**, Xie C, Kotti T, Turley SD, Dietschy JM, Russell DW. J Biol Chem. 2003 Jun 20;278(25):22980-8.
Metabolites in vertebrate Hedgehog signaling. **Roberg-Larsen H**, Strand MF, Krauss S, Wilson SR. Biochem Biophys Res Commun. 2014 Apr 11;446(3):669-74.
The detection of 20S-hydroxycholesterol in extracts of rat brains and human placenta by a gas chromatograph/mass spectrometry technique. **Lin YY**, Welch M, Lieberman S. J Steroid Biochem Mol Biol. 2003 May;85(1):57-61.
Alzheimer disease beta-amyloid activity mimics cholesterol oxidase. **Puglielli L**, Friedlich AL, Setchell KD, Nagano S, Opazo C, Cherny RA, Barnham KJ, Wade JD, Melov S, Kovacs DM, Bush AI. J Clin Invest. 2005 Sep;115(9):2556-63. Epub 2005 Aug 25. Erratum in: J Clin Invest. 2006 Oct;116(10):2828.
Genome-wide atlas of gene expression in the adult mouse brain. **Lein ES**, Hawrylycz MJ, Ao N, Ayres M, Bensinger A, Bernard A, Boe AF, Boguski MS, Brockway KS, Byrnes EJ, Chen L, Chen L, Chen TM, Chin MC, Chong J, Crook BE, Czaplinska A, Dang CN, Datta S, Dee NR, Desaki AL, Desta T, Diep E, Dolbeare TA, Donelan MJ, Dong HW, Dougherty JG, Duncan BJ, Ebbert AJ, Eichele G, Estin LK, Faber C, Facer BA, Fields R, Fischer SR, Fliss TP, Frensley C, Gates SN, Glattfelder KJ, Halverson KR, Hart MR, Hohmann JG, Howell MP, Jeung DP, Johnson RA, Karr PT, Kawal R, Kidney JM, Knapik RH, Kuan CL, Lake JH, Laramee AR, Larsen KD, Lau C, Lemon TA, Liang AJ, Liu Y, Luong LT, Michaels J, Morgan JJ, Morgan RJ, Mortrud MT, Mosqueda NF, Ng LL, Ng R, Orta GJ, Overly CC, Pak TH, Parry SE, Pathak SD, Pearson OC, Puchalski RB, Riley ZL, Rockett HR, Rowland SA, Royall JJ, Ruiz MJ, Sarno NR, Schaffnit K, Shapovalova NV, Sivisay T, Slaughterbeck CR, Smith SC, Smith KA, Smith BI, Sodt AJ, Stewart NN, Stumpf KR, Sunkin SM, Sutram M, Tam A, Teemer CD, Thaller C, Thompson CL, Varnam LR, Visel A,

Whitlock RM, Wohnoutka PE, Wolkey CK, Wong VY, Wood M, Yaylaoglu MB, Young RC, Youngstrom BL, Yuan XF, Zhang B, Zwingman TA, Jones AR. Nature. 2007 Jan 11;445(7124):168-76.
Differential regulation of the human CYP11A1 promoter in mouse brain and adrenals. **Chiang YF**, Lin HT, Hu JW, Tai YC, Lin YC, Hu MC. J Cell Physiol. 2011 Aug;226(8):1998-2005.
Oxysterols are novel activators of the hedgehog signaling pathway in pluripotent mesenchymal cells. **Dwyer JR**, Sever N, Carlson M, Nelson SF, Beachy PA, Parhami F.J Biol Chem. 2007 Mar 23;282(12):8959-68.
Oxysterols are allosteric activators of the oncoprotein Smoothened. **Nachtergaele S**, Mydock LK, Krishnan K, Rammohan J, Schlesinger PH, Covey DF, Rohatgi R. Nat Chem Biol. 2012 Jan 8;8(2):211-20.
Oxysterol binding to the extracellular domain of Smoothened in Hedgehog signaling. **Nedelcu D**, Liu J, Xu Y, Jao C, Salic A. Nat Chem Biol. 2013 Sep;9(9):557-64.
Evaluation of novel derivatisation reagents for the analysis of oxysterols. **Crick PJ**, Aponte J, Bentley TW, Matthews I, Wang Y, Griffiths WJ. Biochem Biophys Res Commun. 2014 Apr 11;446(3):756-61.

Figure Captions

Figure 1. Derivatisation and fragmentation of steroids, sterols and oxysterols. (A) Derivatisation of corticosteroids (corticosterone, R_1 = OH, R_2 = $COCH_2OH$; 11-dehydrocorticosterone, R_1 = O, R_2 = $COCH_2OH$) or testosterone (R_1 = H, R_2 = OH) with Girard T (GT) reagent. (B) Derivatisation of 7-OC with $[^2H_0]$Girard P reagent ($[^2H_0]$GP) and of (C) 24S-HC with $[^2H_5]$GP reagent following enzymatic oxidation with cholesterol oxidase.

Figure 2. Schematic representation of the of the µLESA system linked to with nano-LC. With connections between ports 1 and 6 and between 3 and 2, the 6-port injection valve is in the load position. Once loaded, connections are made between ports 4 and 3 and between 6 and 5. Sample is transported to the 10-port valve and with connections made between ports 8 and 9 and 2 and 3 (on the 10-port valve), sterols are trapped on the C_8 trap-column. Port 1 is then connected to 2, 9 to 10 and sterols eluted from the trap column to the analytical nano-LC column.

Figure 3. µLESA-nano-LC-MS(MS^n) analysis following EADSA treatment of mouse brain. (A) Summed mass spectra recorded over the entire chromatogram from striatum of WT mouse brain. (B) RICs for the $[M]^+$ ion of endogenous 24S-HC (*m/z* 539.4368 ± 10 ppm, upper panel) and sprayed-on $[^2H_7]$24R/S-HC (546.4807 ± 10 ppm, central panel) from striatum of WT mouse brain and endogenous monohydroxycholesterols (*m/z* 539.4368 ± 10 ppm, lower panel) from striatum of *Cyp46a1-/-* mouse brain. The three chromatograms are normalised to the most intense peak in the WT mouse brain. (C) MRM ($[M]^+ \rightarrow [M\text{-}Py]^+ \rightarrow 353.3$) chromatograms for endogenous 24S-HC (upper panel) and sprayed-on $[^2H_7]$24R/S-HC (central panel) from WT mouse and for endogenous 24-HC from *Cyp46a1-/-* mouse. The y-axis is normalised to the most intense peak in each individual chromatogram. In both (B) and (C) the chromatograms have been realigned with reference to elution of the internal standard $[^2H_7]$24R/S-HC. (D) Mass spectrum recorded at 27.57 min from the striatum of WT mouse. (E) MS^3 ($[M]^+ \rightarrow [M\text{-}Py]^+ \rightarrow$) spectra recorded at 27.52 min corresponding to endogenous 24S-HC (upper panel) and 27.44 min corresponding to sprayed-on $[^2H_7]$24S-HC (lower panel) from striatum of WT mouse. Note that 24S-HC appears as a doublet in the chromatograms (B) and (C), this is a consequence of *syn* and *anti* conformers of the GP-derivative. Similarly, each of the R and S epimers of the $[^2H_7]$24R/S-HC mixture give *syn* and *anti* conformers which are partially resolved. Shown in Supplemental Figure S4A is the RIC for the $[M]^+$ ion of cholesterol (*m/z* 523.4419 ± 10 ppm, WT mouse upper panel) and for monohydroxycholesterols (*m/z* 539.4368 ± 10 ppm, WT mouse central panel, *Cyp46a1-/-* mouse lower panel), including cholesterol autoxidation products, from the striatum. The *ex vivo* autoxidation products elute considerably later than endogenous side-chain hydroxycholesterols. All three panels are shown on the same y-axis

Figure 4. Sagittal section of WT mouse brain analysed by µLESA-nano-LC-MS following EADSA treatment. (A) Areal density of 24S-HC in four nearby sagittal slices cut from a single brain. (B) Areal density of 24S-HC in six nearby slices cut from three different brains. Slices were taken from the right hemisphere 1 – 2 mm away from the midsagittal line. The number of spots analysed for each region of each brain slice is indicated by numbers within the bars. %CV is shown above the bars for each region. (C) The Table shows values for areal density, across the six slices for the three mice (WT-1 – WT-3) and nine different brain regions. Average areal density and SD is calculated from data for the six slices. Data is converted into ng/mg-brain based on a brain-mass/area ratio of 0.0102 mg/mm^2 for a typical brain slice. (D) Images of the sagittal section of WT mouse brain analysed by µLESA-nano-LC-MS. The top panel shows a photograph of a tissue slice from WT mouse brain showing spots analysed with areal density, determined by µLESA-nano-LC-MS, of 24S-HC colour coded on a blue to red scale. The lower panel shows a Luxol Fast Blue and Cresyl Violet stained brain slice, adjacent to the slice analysed by µLESA-nano-LC-MS, with areal density of 24S-HC colour coded as in the upper panel.

Figure 5. Sagittal section of mouse brain analysed by µLESA-nano-LC-MS following EADSA treatment. (A) Areal density of 24S-HC in the nine brain regions from the three WT mice. (B) Areal density for the combination of 3β,7α-diHCA and 7αH,3O-CA in the nine brain regions from the three WT mice. (C) Areal density of 24R-HC in the nine different brain regions from three *Cyp46a1-/-* mice. Statistical differences between the nine regions for the three biological replicates are indicated. The number of spots analysed for each brain region is indicated within the bars.

Figure 6. MALDI-MSI following EADSA treatment of a sagittal section of WT brain. (A) Image of the $[M]^+$ ion of cholesterol. (B) Different regions of mouse brain [Lein 2007]. Image credit: Allen Institute. http://mouse.brain-map.org/experiment/thumbnails/100042147?image_type=atlas.

Figure 1

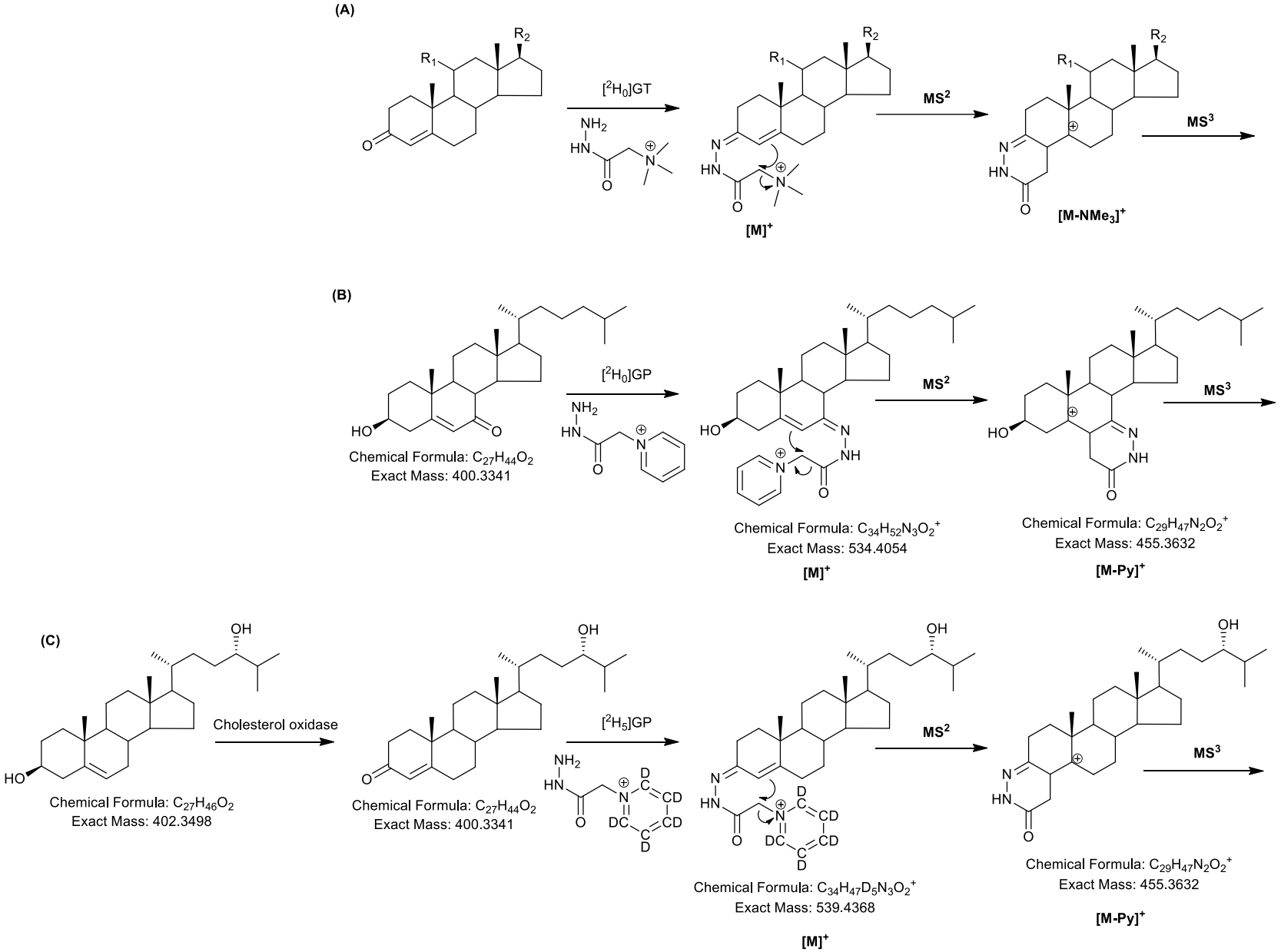
(A)
R1
R2
[2H0]GT
NH2
HN
O
N
MS2
MS3
[M]+
[M-NMe3]+
(B)
HO
[2H0]GP
Chemical Formula: C27H44O2
Exact Mass: 400.3341
NH
Chemical Formula: C34H52N3O2+
Exact Mass: 534.4054
[M]+
Chemical Formula: C29H47N2O2+
Exact Mass: 455.3632
[M-Py]+
(C)
OH
Cholesterol oxidase
Chemical Formula: C27H46O2
Exact Mass: 402.3498
[2H5]GP
D
CD
DC
Chemical Formula: C34H47D5N3O2+
Exact Mass: 539.4368
[M]+

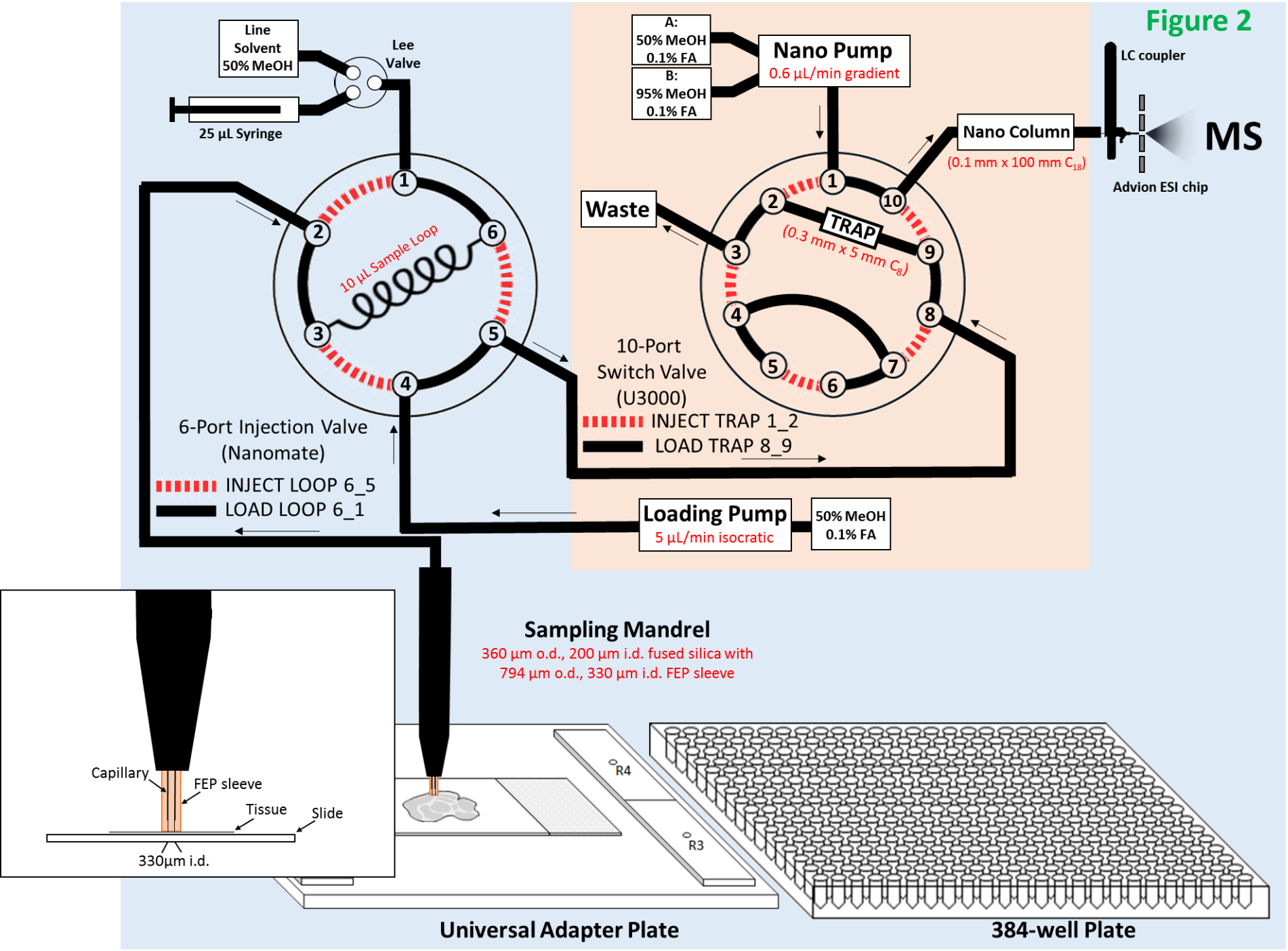
Figure 2
Line Solvent 50% MeOH
Lee Valve
25 µL Syringe
A: 50% MeOH 0.1% FA
B: 95% MeOH 0.1% FA
Nano Pump
0.6 µL/min gradient
LC coupler
Nano Column
(0.1 mm x 100 mm C18)
MS
Advion ESI chip
Waste
TRAP
(0.3 mm x 5 mm C8)
10 µL Sample Loop
10-Port Switch Valve (U3000)
INJECT TRAP 1_2
LOAD TRAP 8_9
6-Port Injection Valve (Nanomate)
INJECT LOOP 6_5
LOAD LOOP 6_1
Loading Pump
5 µL/min isocratic
50% MeOH 0.1% FA
Sampling Mandrel
360 µm o.d., 200 µm i.d. fused silica with
794 µm o.d., 330 µm i.d. FEP sleeve
Capillary
FEP sleeve
Tissue
Slide
330µm i.d.
R4
R3
Universal Adapter Plate
384-well Plate

Figure 3A

EY_180907_MAST_WT-4_#55_withCO_striat... 09/09/18 14:04:58

EY_180907_MAST_WT-4_#55_withCO_striatum2_[C8_02_trap]_Nano-01_ ı-15999 RT: 2.24-50.00 AV: 1142 NL: 1.28E7

F: FTMS + p NSI Full ms [400.00-610.00]

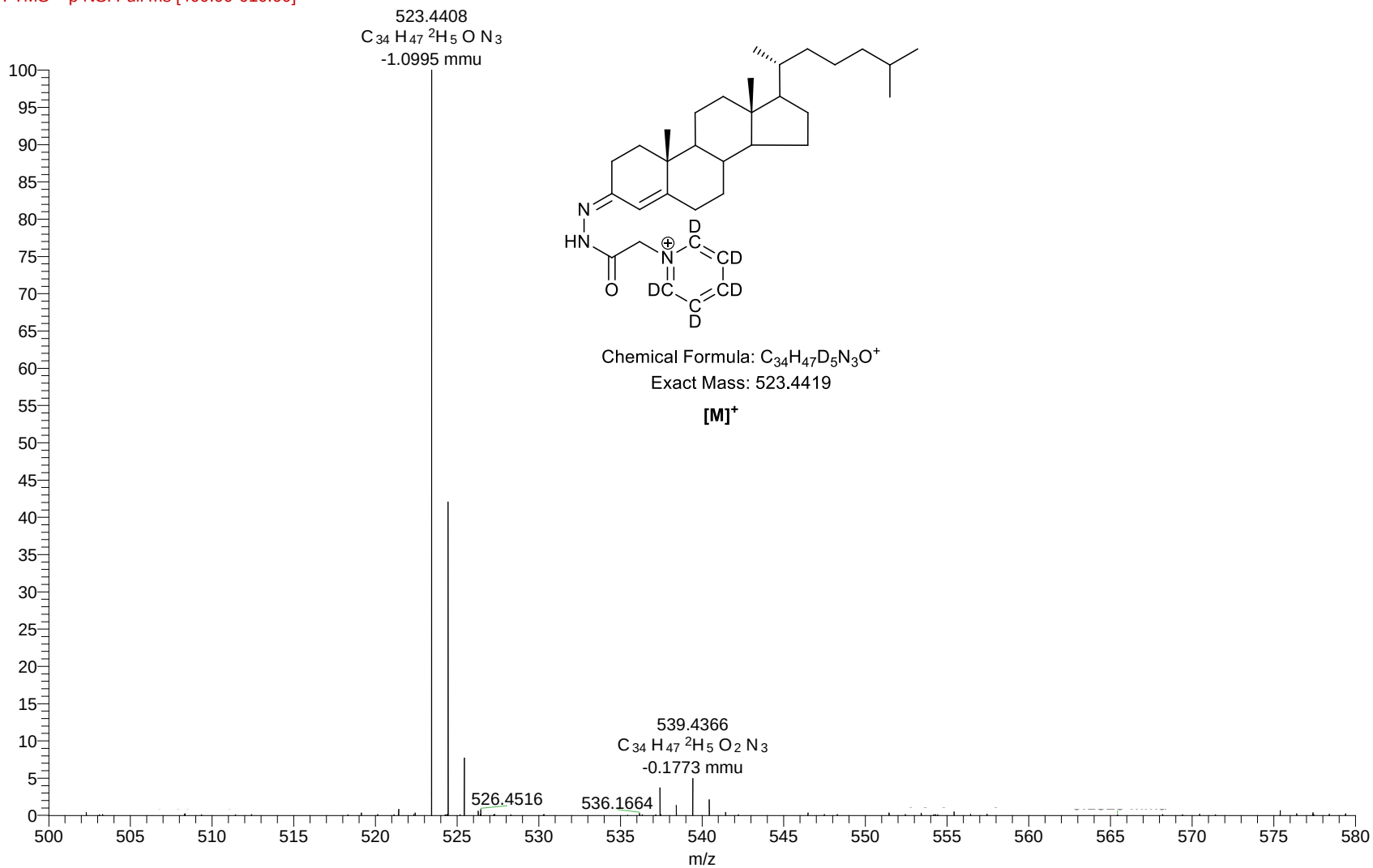

Chemical Formula: $C_{34}H_{47}D_5N_3O^+$

Exact Mass: 523.4419

$[M]^+$

Figure 3B

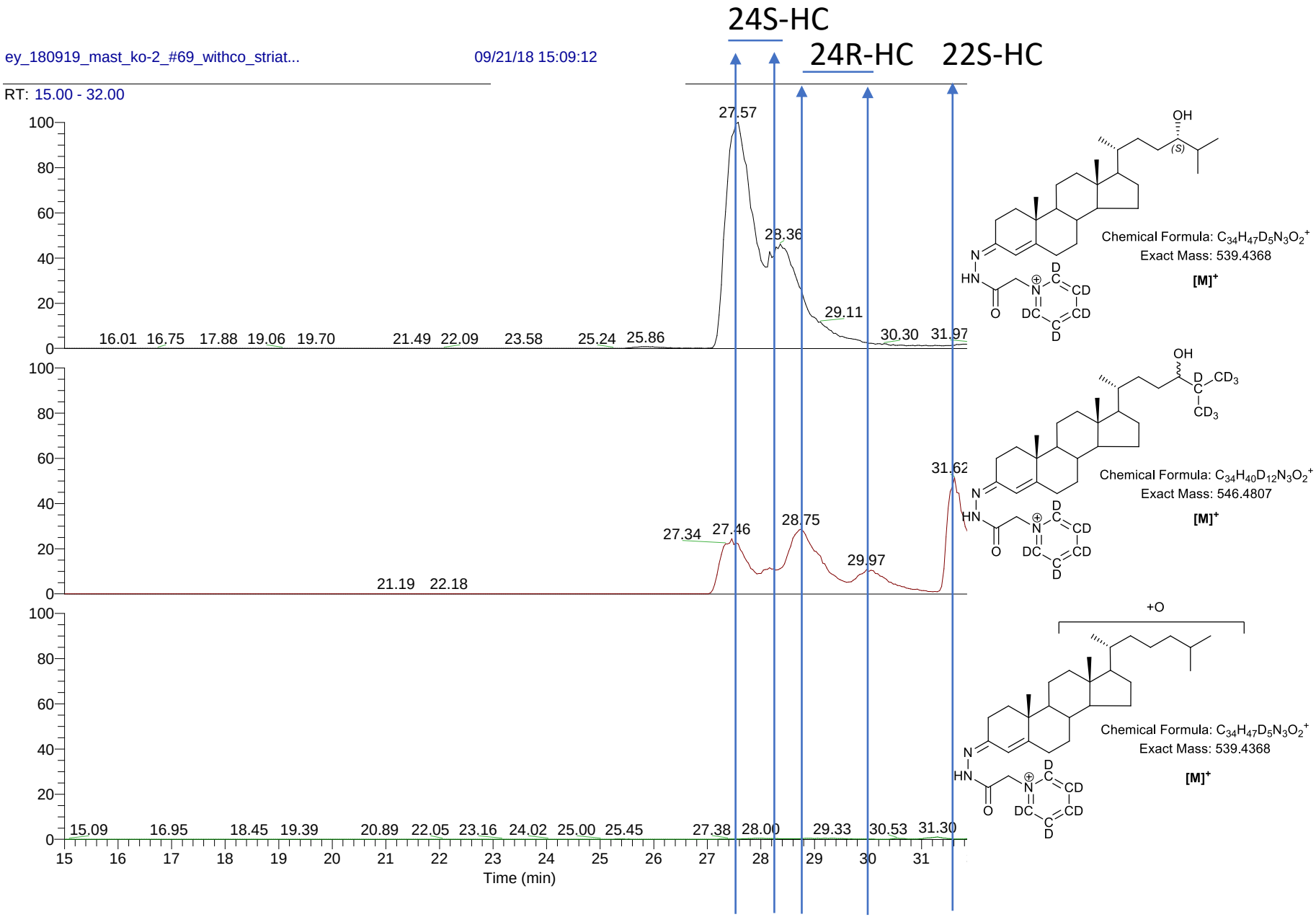
24S-HC
24R-HC
22S-HC
ey_180919_mast_ko-2_#69_withco_striat...
09/21/18 15:09:12
RT: 15.00 - 32.00
27.57
28.36
29.11
30.30
31.97
16.01
16.75
17.88
19.06
19.70
21.49
22.09
23.58
25.24
25.86
31.62
27.34
27.46
28.75
29.97
21.19
22.18
15.09
16.95
18.45
19.39
20.89
22.05
23.16
24.02
25.00
25.45
27.38
28.00
29.33
30.53
31.30
Time (min)
Chemical Formula: C34H47D5N3O2+
Exact Mass: 539.4368
[M]+
Chemical Formula: C34H40D12N3O2+
Exact Mass: 546.4807
[M]+
+O
Chemical Formula: C34H47D5N3O2+
Exact Mass: 539.4368
[M]+

Figure 3C

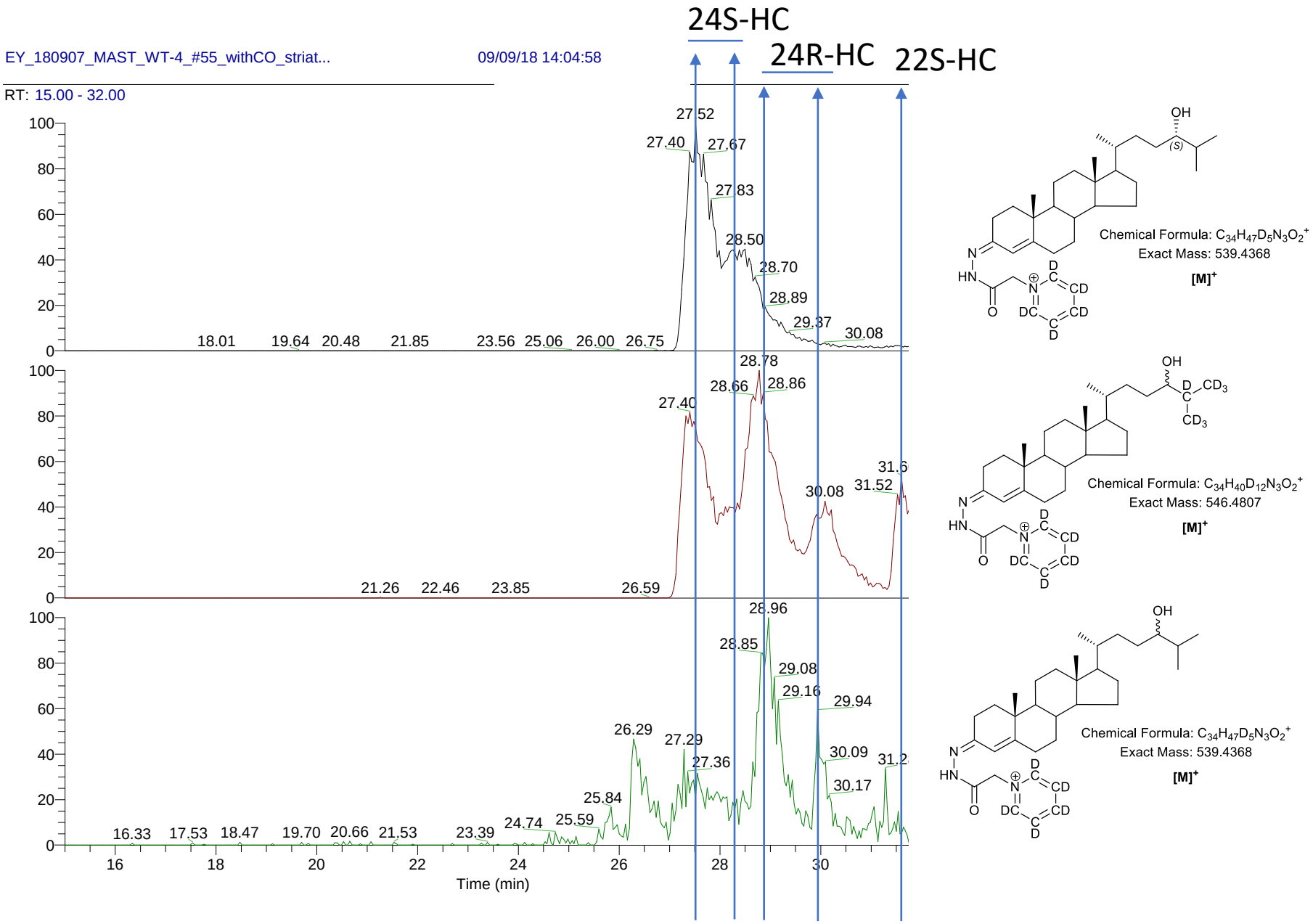
24S-HC
24R-HC
22S-HC
EY_180907_MAST_WT-4_#55_withCO_striat...
09/09/18 14:04:58
RT: 15.00 - 32.00
Time (min)
Chemical Formula: $C_{34}H_{47}D_5N_3O_2^+$
Exact Mass: 539.4368
$[M]^+$
Chemical Formula: $C_{34}H_{40}D_{12}N_3O_2^+$
Exact Mass: 546.4807
$[M]^+$
Chemical Formula: $C_{34}H_{47}D_5N_3O_2^+$
Exact Mass: 539.4368
$[M]^+$

Figure 3D

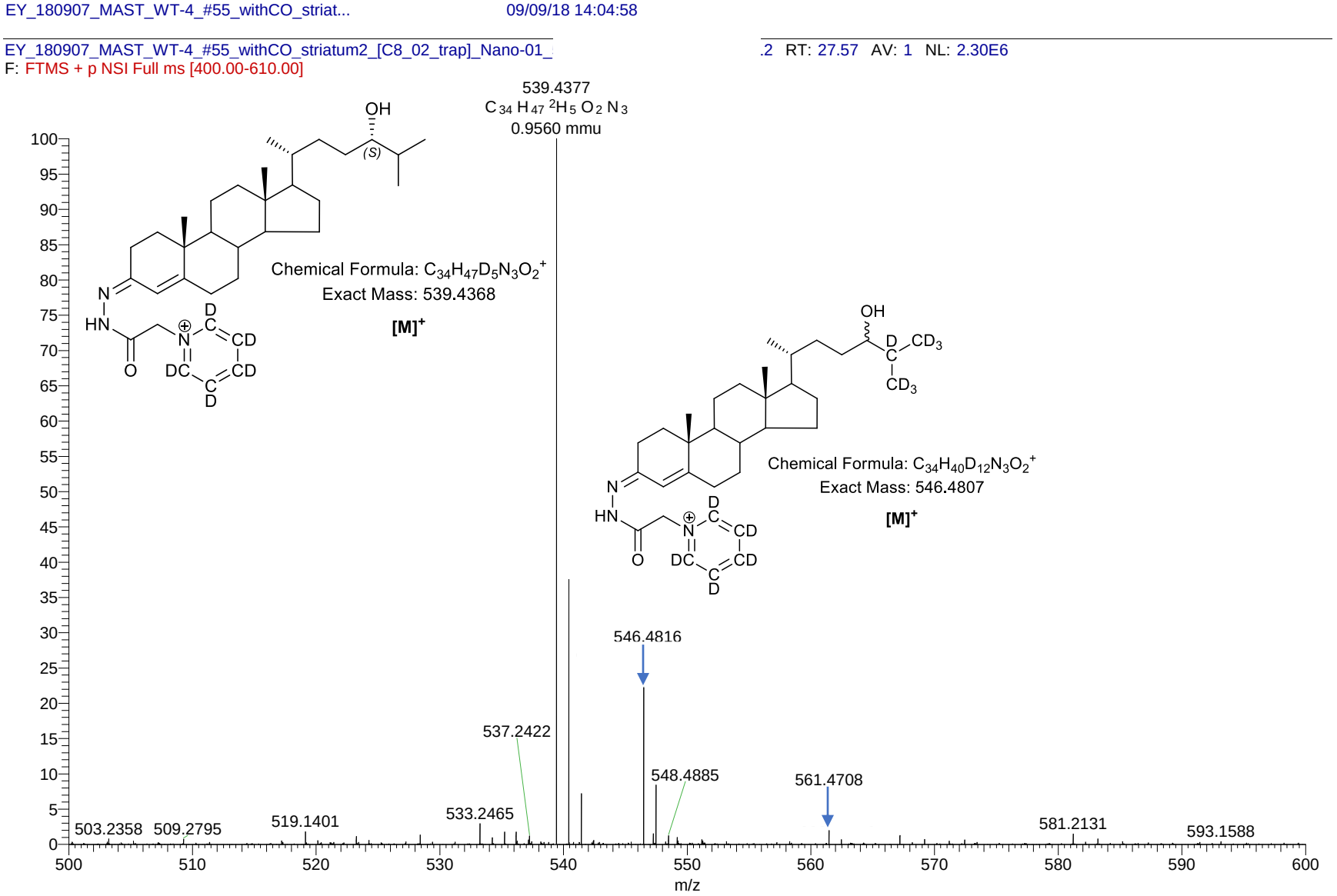
EY_180907_MAST_WT-4_#55_withCO_striat...
09/09/18 14:04:58
EY_180907_MAST_WT-4_#55_withCO_striatum2_[C8_02_trap]_Nano-01_
.2 RT: 27.57 AV: 1 NL: 2.30E6
F: FTMS + p NSI Full ms [400.00-610.00]
539.4377
C 34 H 47 2H 5 O 2 N 3
0.9560 mmu
Chemical Formula: C34H47D5N3O2+
Exact Mass: 539.4368
[M]+
Chemical Formula: C34H40D12N3O2+
Exact Mass: 546.4807
[M]+
546.4816
537.2422
548.4885
561.4708
503.2358
509.2795
519.1401
533.2465
581.2131
593.1588
m/z

Figure 3E

EY_180907_MAST_WT-4_#55_withCO_striat... 09/09/18 14:04:58

EY_180907_MAST_WT-4_#55_withCO_striat
F: ITMS + c NSI Full ms3 539.44@cid30.00 4
_55min_1'7kV_300ct_50 #5199 RT: 27.52 AV: 1 NL: 1.51E5
.00]

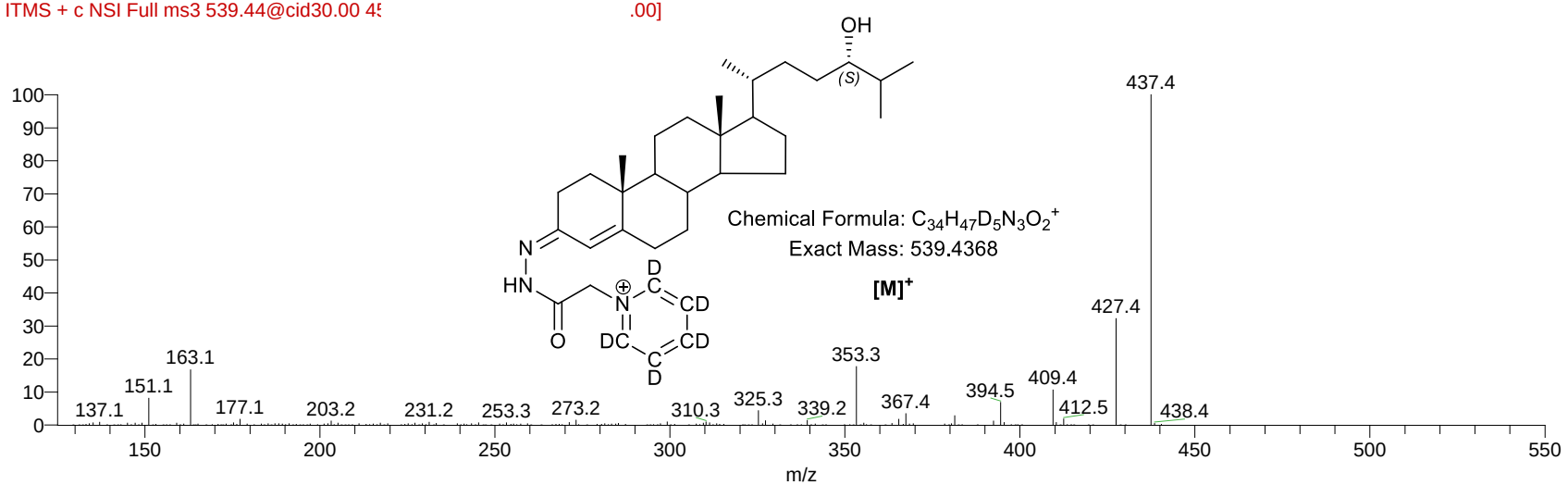

EY_180907_MAST_WT-4_#55_withCO_striatum2_[C8_02_trap]_Nano-01_55min_1'7kV_300ct_50 #5182 RT: 27.44 AV: 1 NL: 4.25E4
F: ITMS + c NSI Full ms3 546.48@cid30.00 462.41@cid35.00 [125.00-555.00]

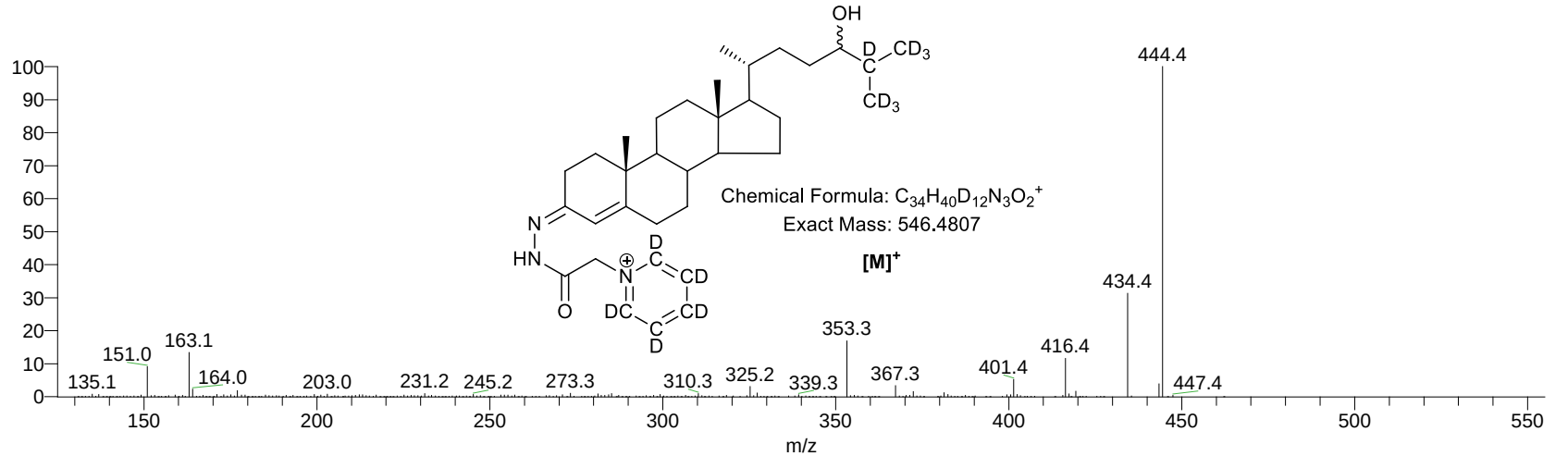

Figure 4A

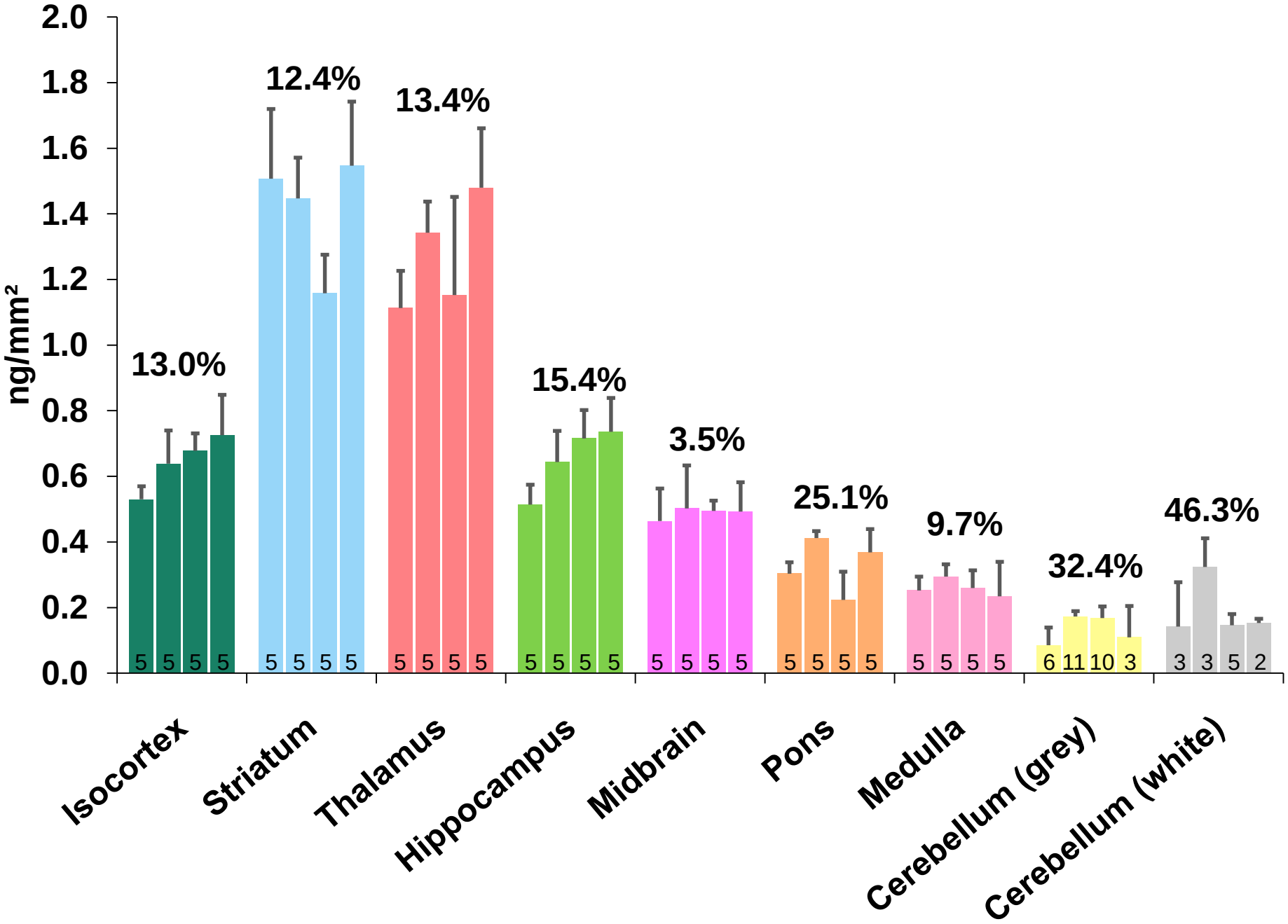
ng/mm²
2.0
1.8
1.6
1.4
1.2
1.0
0.8
0.6
0.4
0.2
0.0
13.0%
12.4%
13.4%
15.4%
3.5%
25.1%
9.7%
32.4%
46.3%
5 5 5 5
5 5 5 5
5 5 5 5
5 5 5 5
5 5 5 5
5 5 5 5
5 5 5 5
6 11 10 3
3 3 5 2
Isocortex
Striatum
Thalamus
Hippocampus
Midbrain
Pons
Medulla
Cerebellum (grey)
Cerebellum (white)

Figure 4B

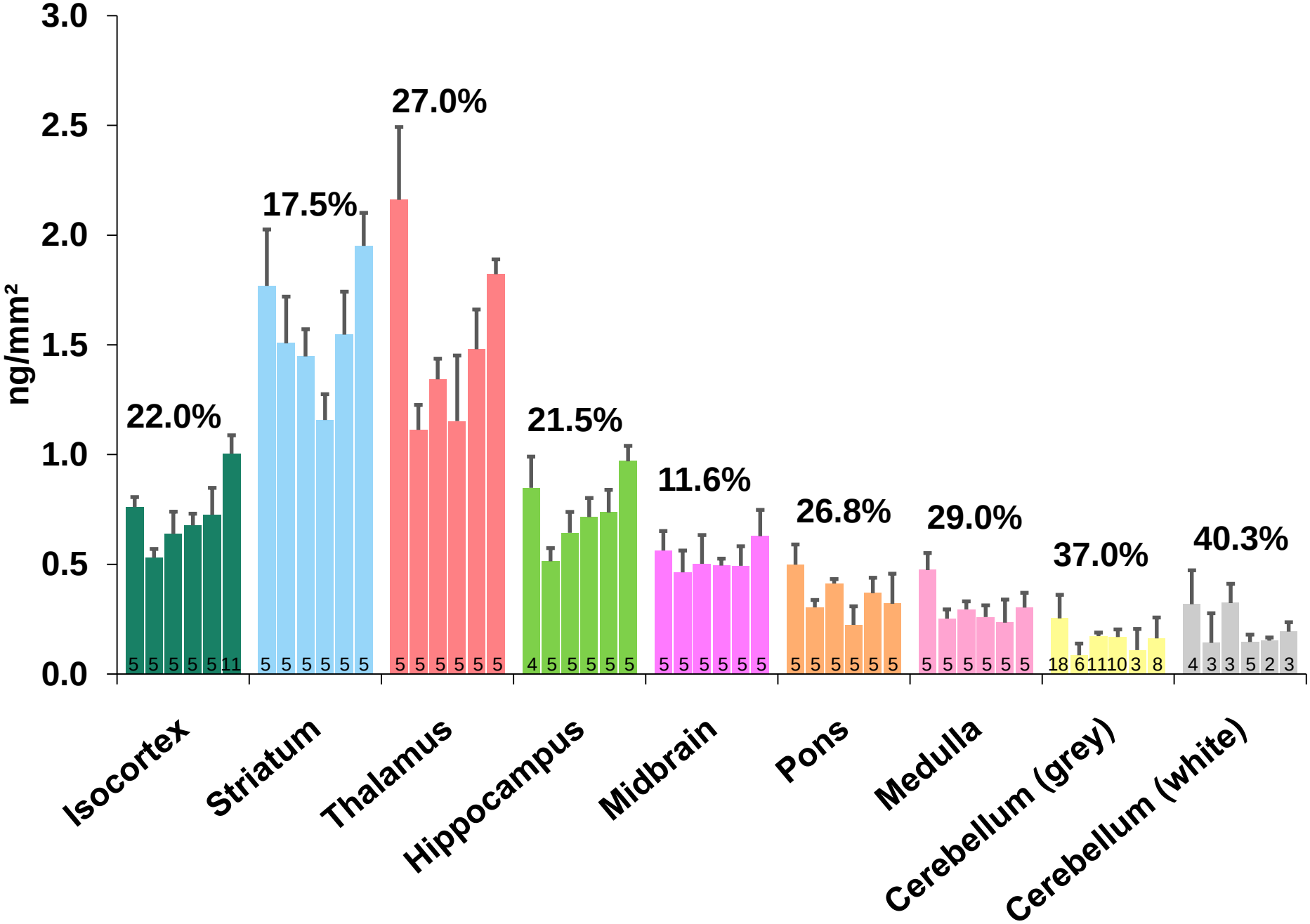
3.0
2.5
2.0
1.5
1.0
0.5
0.0
ng/mm²
22.0%
17.5%
27.0%
21.5%
11.6%
26.8%
29.0%
37.0%
40.3%
5 5 5 5 5 11
5 5 5 5 5 5
5 5 5 5 5 5
4 5 5 5 5 5
5 5 5 5 5 5
5 5 5 5 5 5
5 5 5 5 5 5
18 6 11 10 3 8
4 3 3 5 2 3
Isocortex
Striatum
Thalamus
Hippocampus
Midbrain
Pons
Medulla
Cerebellum (grey)
Cerebellum (white)

Figure 4C

WT	24S-HC								
	Tissue Slice Areal Density ng/mm^2						Average Areal Density (ng/mm^2)	SD	Average concentration (ng/mg-brain)
	WT-1	WT-3	WT-3	WT-3	WT-3	WT-4			
Isocortex	0.76	0.53	0.64	0.68	0.73	1.00	0.72	0.16	70.42
Striatum	1.77	1.51	1.45	1.16	1.55	1.95	1.56	0.27	152.30
Thalamus	2.16	1.11	1.34	1.15	1.48	1.82	1.51	0.41	147.32
Hippocampus	0.85	0.51	0.64	0.72	0.74	0.97	0.74	0.16	71.88
Midbrain	0.56	0.46	0.50	0.49	0.49	0.63	0.52	0.06	51.06
Pons	0.50	0.30	0.41	0.22	0.37	0.32	0.35	0.10	34.53
Medulla	0.47	0.25	0.29	0.26	0.23	0.30	0.30	0.09	29.52
Cerebellum (grey)	0.25	0.09	0.17	0.17	0.11	0.16	0.16	0.06	15.46
Cerebellum (white)	0.32	0.14	0.32	0.15	0.15	0.19	0.21	0.09	20.73

Figure 4D

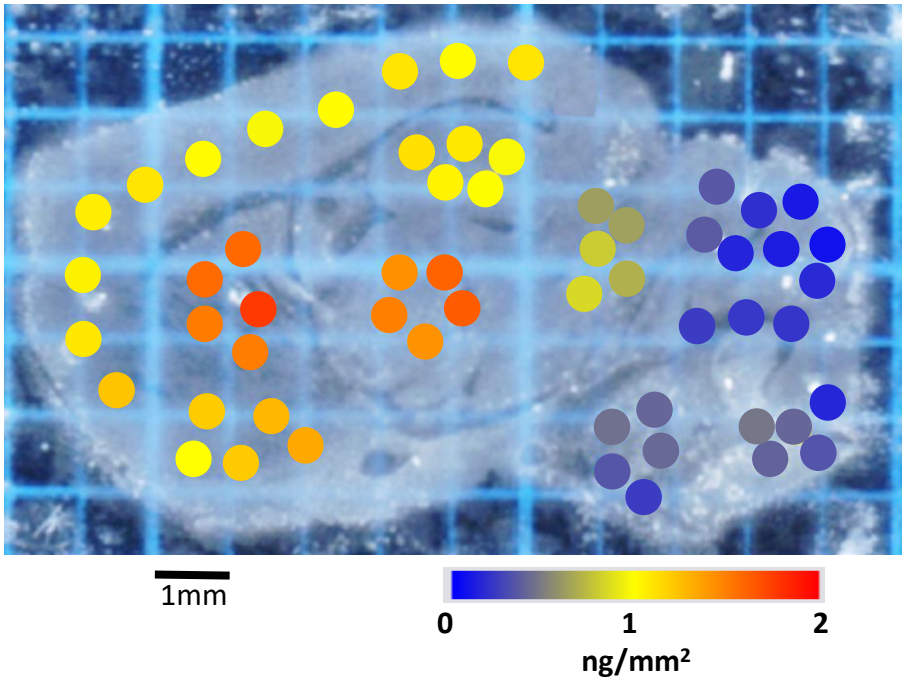

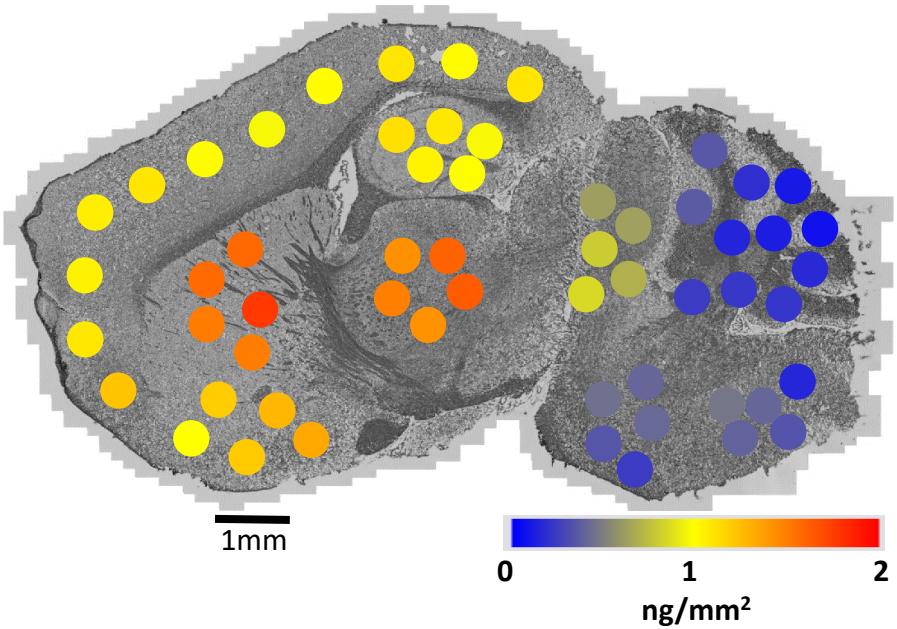

Figure 5A

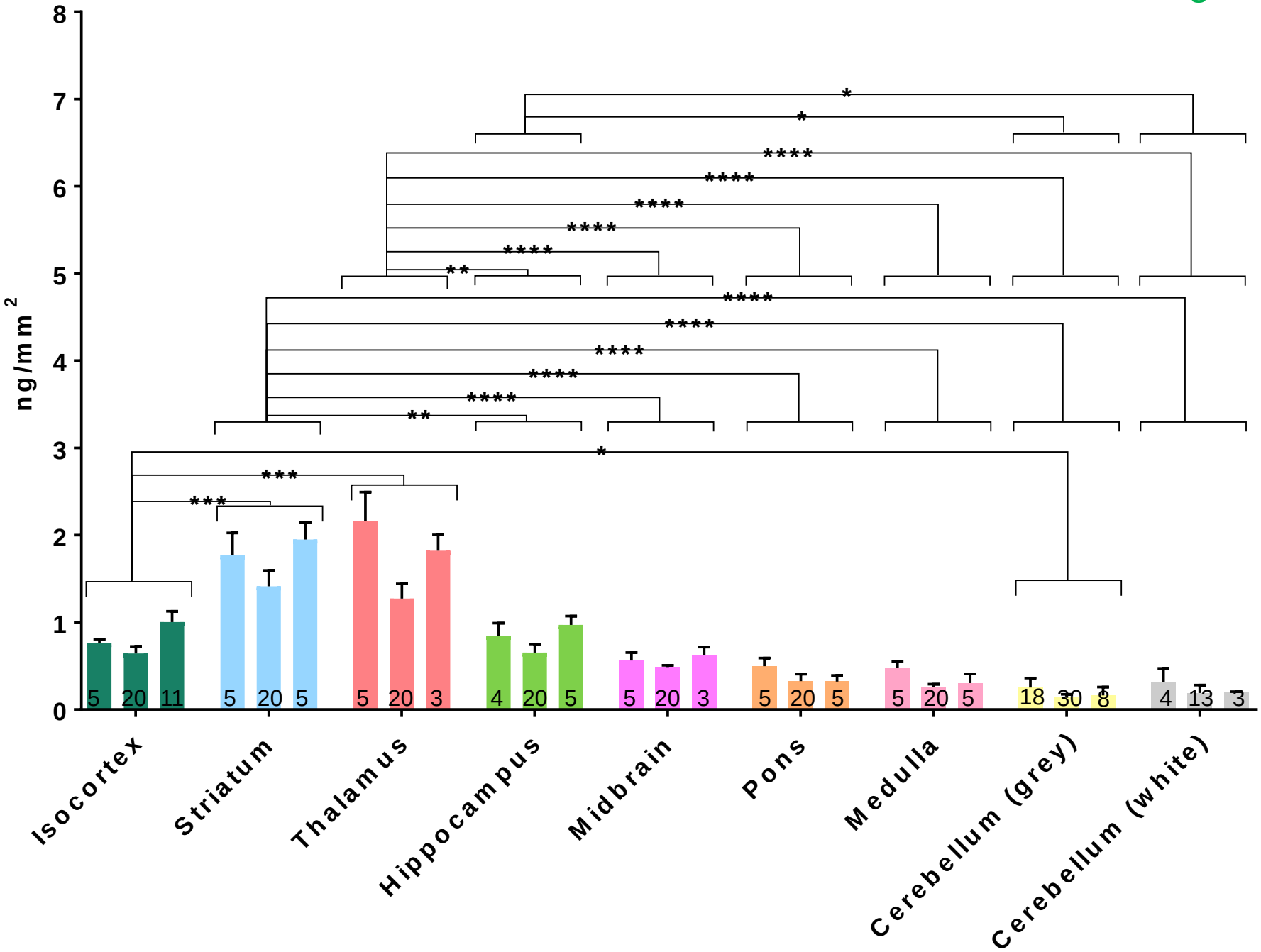
ng/mm 2
0
1
2
3
4
5
6
7
8
*
*
****
****
****
****
****
**
****
****
****
****
****
**
*
***
***
5
20
11
5
20
5
5
20
3
4
20
5
5
20
3
5
20
5
5
20
5
18
30
8
4
13
3
Isocortex
Striatum
Thalamus
Hippocampus
Midbrain
Pons
Medulla
Cerebellum (grey)
Cerebellum (white)

Figure 5B

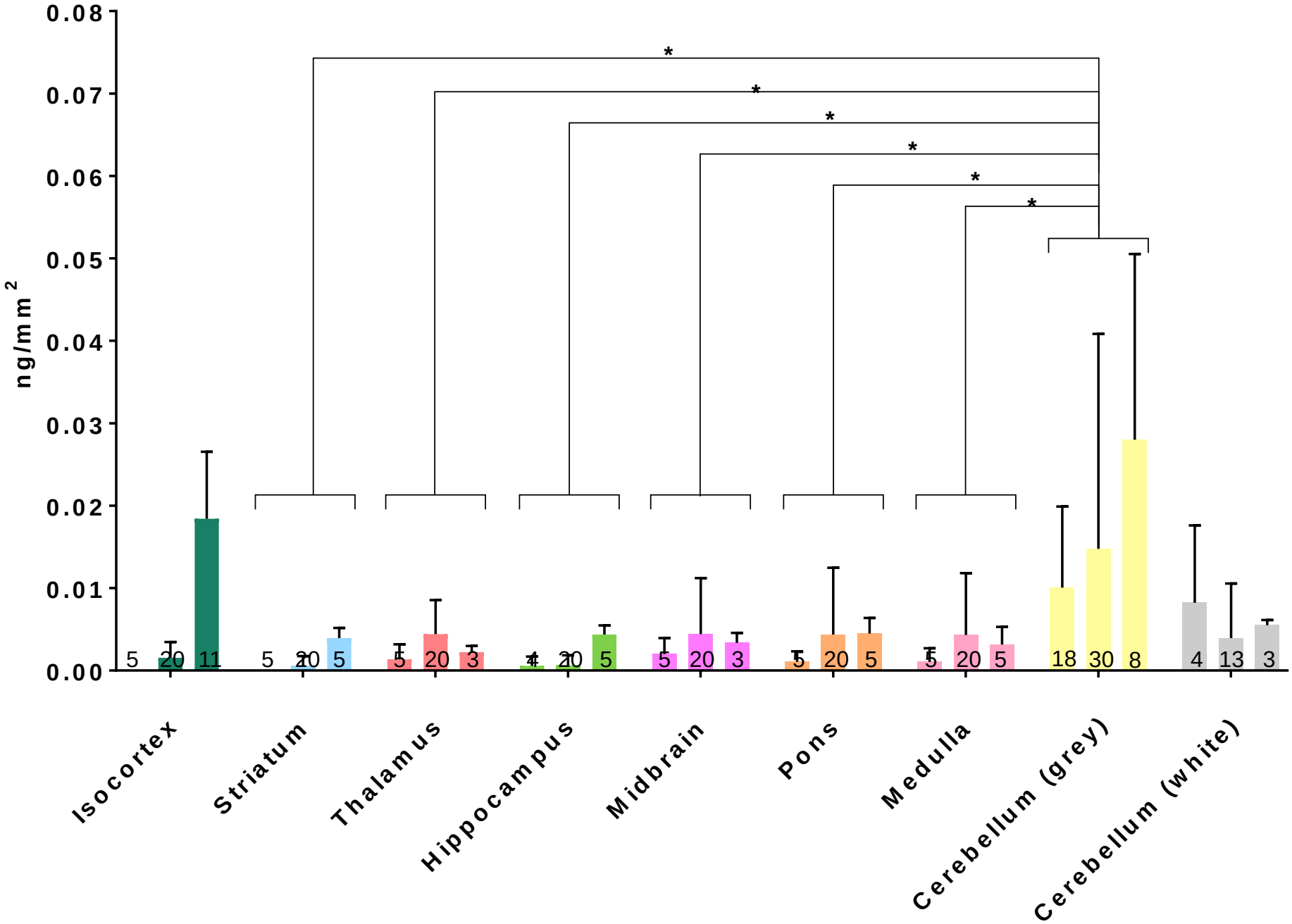
0.08
0.07
0.06
0.05
0.04
0.03
0.02
0.01
0.00
ng/mm2
*
*
*
*
*
*
5
20
11
5
20
5
5
20
3
4
20
5
5
20
3
5
20
5
5
20
5
18
30
8
4
13
3
Isocortex
Striatum
Thalamus
Hippocampus
Midbrain
Pons
Medulla
Cerebellum (grey)
Cerebellum (white)

Figure 5C

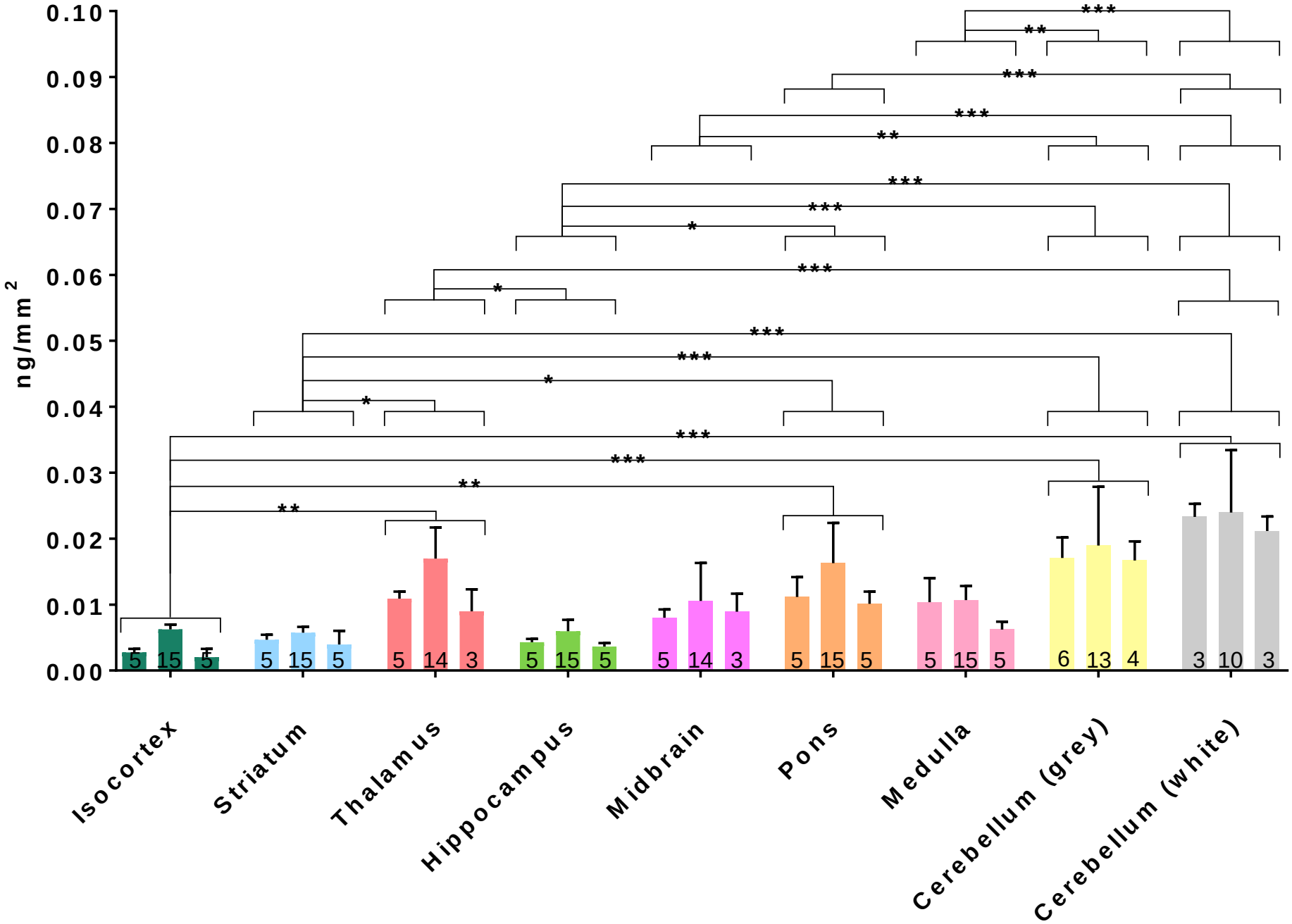
0.10
0.09
0.08
0.07
0.06
0.05
0.04
0.03
0.02
0.01
0.00
ng/mm2
***
**
***
***
**
***
***
*
***
*
***
***
*
*
***
***
**
**
5 15 5
5 15 5
5 14 3
5 15 5
5 14 3
5 15 5
5 15 5
6 13 4
3 10 3
Isocortex
Striatum
Thalamus
Hippocampus
Midbrain
Pons
Medulla
Cerebellum (grey)
Cerebellum (white)

Figure 6

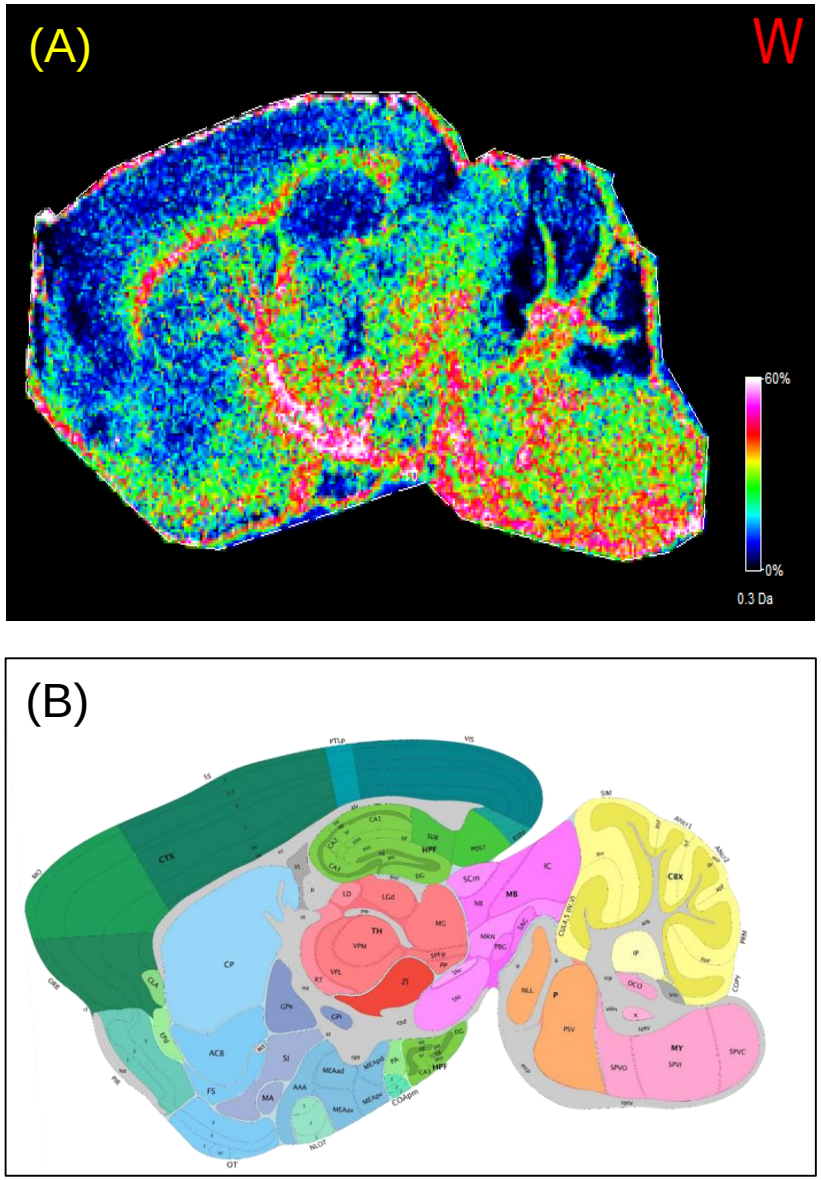
(A)
W
60%
0%
0.3 Da
(B)
CTX
CP
ACB
FS
MA
SI
HPF
TH
VPM
VPL
ZI
MG
MB
IC
CBX
P
PSV
MY
SPVO
SPVI
SPVC
NLL
DCO
IP
SCm
NB
LD
LGd
GPe
GPi
MEAad
MEAav
MEApd
MEApv
COApm
NLOT
OT
PTLp
VIS
SS
MO
SIM
ANtr1
ANtr2
PRM
COPY
CLA
EPd
ORB
PIR
CA1
CA2
CA3
SUB
POST
DG
RT
PA
SAG
MRN
PBG
SPFp
PP
SNr
CUEAS (IV-V)
X
NPV
SPVI
SPVO
SPVC